Monthly Notices
of the
ROYAL ASTRONOMICAL SOCIETY

MNRAS **440,** 1934–1949 (2014) doi:10.1093/mnras/stu389

Quenching star formation in cluster galaxies

Dan S. Taranu,[1,2⋆] Michael J. Hudson,[2,3] Michael L. Balogh,[2,4] Russell J. Smith,[5] Chris Power,[6,7] Kyle A. Oman[2,8] and Brad Krane[2]

[1]*Department of Astronomy and Astrophysics, University of Toronto, 50 St. George Street, Toronto, ON M5S 3H4, Canada*
[2]*Department of Physics and Astronomy, University of Waterloo, 200 University Avenue West, Waterloo, ON N2L 3G1, Canada*
[3]*Perimeter Institute for Theoretical Physics, 31 Caroline St. N., Waterloo, ON N2L 2Y5, Canada*
[4]*Leiden Observatory, Leiden University, PO Box 9513, NL-2300 RA Leiden, the Netherlands*
[5]*Department of Physics, University of Durham, Science Laboratories, South Road, Durham DH1 3LE, UK*
[6]*International Centre for Radio Astronomy Research, The University of Western Australia, 35 Stirling Highway, Crawley, WA 6009, Australia*
[7]*ARC Centre of Excellence for All-Sky Astrophysics (CAASTRO), Redfern, NSW 2016, Australia*
[8]*Department of Physics and Astronomy, University of Victoria, Victoria, BC V8P 5C2, Canada*

Accepted 2014 February 26. Received 2014 February 25; in original form 2013 November 25

ABSTRACT

In order to understand the processes that quench star formation in cluster galaxies, we construct a library of subhalo orbits drawn from Λ cold dark matter cosmological *N*-body simulations of four rich clusters. We combine these orbits with models of star formation followed by environmental quenching, comparing model predictions with observed bulge and disc colours and stellar absorption line-strength indices of luminous cluster galaxies. Models in which the bulge stellar populations depend only on the galaxy subhalo mass while the disc is quenched upon infall are acceptable fits to the data. An exponential disc quenching time-scale of 3–3.5 Gyr is preferred. Quenching in lower mass groups prior to infall ('pre-processing') provides better fits, with similar quenching time-scales. Models with short ($\lesssim$1 Gyr) quenching time-scales yield excessively steep cluster-centric gradients in disc colours and Balmer line indices, even if quenching is delayed for several Gyr. The data slightly prefer models where quenching occurs only for galaxies falling within $\sim 0.5 r_{200}$. These results imply that the environments of rich clusters must impact star formation rates of infalling galaxies on relatively long time-scales, indicative of gentler quenching mechanisms such as slow 'strangulation' over more rapid ram-pressure stripping.

Key words: galaxies: clusters: general – galaxies: evolution – galaxies: formation – galaxies: haloes – galaxies: star formation – galaxies: stellar content.

1 INTRODUCTION

Understanding the physical mechanisms that halt star formation in galaxies has been a long-standing challenge in galaxy formation and evolution. It is clear from the colour–magnitude relation (Sandage & Visvanathan 1978; Bower, Lucey & Ellis 1992) that mass or, more accurately, velocity dispersion (Graves, Faber & Schiavon 2009; Smith, Lucey & Hudson 2009b) is a driving parameter of the stellar populations in red galaxies. At the same time, the morphology–density (Hubble & Humason 1931; Dressler 1980; Postman & Geller 1984), the colour–density (Balogh et al. 2004; Hogg et al. 2004) and the age–density (Smith et al. 2006) relations are strong evidence of the role of environment. The latter suggest that environment somehow contributes to 'quenching' star formation, moving galaxies from the blue cloud to the red sequence. Quenching can be abrupt or even instantaneous, as in dousing a fire, or it can operate on longer time-scales. It has become common to model both an 'internal' quenching mechanism (assumed to be tied to galaxy mass) as well as environmental quenching, associated with a galaxy falling into a higher mass halo and becoming a satellite (Kauffmann, White & Guiderdoni 1993; Cole et al. 2000; van den Bosch et al. 2008; Weinmann et al. 2009; Peng et al. 2010, 2012; Wetzel et al. 2013).

Many mechanisms that might quench star formation in cluster environments have been proposed: ram-pressure stripping of the cold gas (Gunn & Gott 1972; Abadi, Moore & Bower 1999), the removal of the hot gas halo (Larson, Tinsley & Caldwell 1980), sometimes known as 'strangulation' (Balogh & Morris 2000) either via ram-pressure (McCarthy et al. 2008) or via tidal stripping by the cluster potential (Merritt 1984; Mamon 1987), or by 'harassment' – encounters with other galaxies (Gallagher & Ostriker 1972; Moore, Lake & Katz 1998). The ram-pressure stripping and strangulation mechanisms remove the gas that is the fuel for star formation, and

⋆ E-mail: taranu@astro.utoronto.ca

so the stellar disc will dim and redden as its stars age. Several of the processes affecting late-type galaxies have been reviewed by Boselli & Gavazzi (2006).

It has long been known that spiral galaxies in the cores of rich clusters are deficient in H I (Davies & Lewis 1973; Haynes, Giovanelli & Chincarini 1984; Giovanelli & Haynes 1985; Solanes et al. 2001) and stripping of star-forming gas has been observed in nearby rich clusters (Koopmann & Kenney 2004; Chung et al. 2007; Sun, Donahue & Voit 2007; Yagi et al. 2007; Yoshida et al. 2008; Sivanandam, Rieke & Rieke 2010; Smith et al. 2010). This stripping usually appears to occur on short (several hundred Myr) time-scales, but it is unclear if this is the dominant quenching mechanism. Other, less abrupt or 'gentler' mechanisms such as strangulation or tidal stripping are more difficult to observe directly. To determine which mechanisms are dominant, one might instead tackle the following more empirical questions: At what location in the cluster or group does quenching first occur? What is the time-scale of quenching – is quenching abrupt, ending all star formation within tens of millions of years, or does star formation slowly declines over billions of years? What range of satellite galaxy masses are effectively quenched by the environment? Are all morphological components quenched equally, or, for example, are bulges insensitive to environment while discs are quenched?

A common approach to understanding these processes is semi-analytic modelling (SAMs for short; see Baugh 2006 for a review). SAMs attempt to model important physical process via analytical prescriptions, combining these with results (e.g. merger trees) from numerical experiments like *N*-body simulations. A disadvantage of the SAM approach when applied to all galaxy populations is that it is difficult to isolate and study specific environments and physical processes, particularly with a large number of potentially correlated free parameters and physical processes. It is also challenging to determine if the parametrizations of physical processes are themselves appropriate. An alternative approach is to apply only a minimal number of physically motivated prescriptions relevant to a specific environment, rather than all possible environments. We choose to focus on the cluster environment. Hudson et al. (2010) have shown that cluster galaxies have bulge fractions and bulge properties which are largely independent of environment and dependent only on internal structure of the galaxy, and that environmental trends are driven by variations in properties of the disc. This forms the basis of our simple model for quenching, outlined below.

In this paper, we will examine the link between star formation rates (SFR) and the cluster environment by combining *N*-body simulations of rich clusters with star formation models. Previous models of galaxy evolution in clusters (Balogh, Navarro & Morris 2000; Diaferio et al. 2001, and references therein) employed models linking SFR with gas consumption, and in some cases, replenishment (Weinmann et al. 2010). More recent studies (Berrier et al. 2009; McGee et al. 2009; De Lucia et al. 2012; Smith et al. 2012) have focused on pre-processing in galaxy groups. While these approaches have been successful in reproducing SFR and colour gradients, they have not yet isolated the mechanism responsible for halting star formation despite including a wide variety of models for physical processes. We instead seek to produce models that employ an easily tested causal connection between environment (traced by infall into a rich cluster) and the evolution of an individual galaxy (see Mahajan, Mamon & Raychaudhury 2011, for a recent example of star formation models of cluster galaxies).

In our models, galaxies (or components thereof such as the bulge and disc) are assumed to be forming stars until quenched by one of two mechanisms. In one scenario, 'internal' quenching of star formation occurs at a time which is assumed to be a function of a galaxy's internal properties (specifically velocity dispersion), such that galaxies with high velocity dispersions are quenched earlier (see Section 4.3.1 for details of our particular implementation). In the alternative scenario, environmental quenching of star formation occurs in the galaxy when its halo crosses some fraction of the virial radius of the cluster, with an option to delay quenching until the galaxy reaches pericentre or for some fixed time after infall. Though these prescriptions depict a simplified view of galaxy evolution, testing models based upon these mechanisms should provide clues as to the relative importance of environments in star formation. Varying the quenching radius of the cluster and allowing quenching to occur in smaller, group-sized haloes ('pre-processing') will also help to determine where quenching is likely to occur.

Most models to date have compared predictions with observations of galaxy luminosities and colours. We aim to compare our models not just with total galaxy colours – which are very red for most cluster galaxies – but also with disc colours, which are more sensitive to star formation models and thus better discriminants of quenching models. We also provide predictions of spectroscopic absorption line-strength indices, which help to break the well-known degeneracies between age, metallicity and α-element enhancement. In this paper, we focus on colour and absorption line-strength data from the NOAO Fundamental Plane Survey (Smith et al. 2004, hereafter NFPS) of galaxies in rich clusters, as well as bulge-disc decompositions (Simard et al. 2011) based on Sloan Digital Sky Survey Data Release 7 data (SDSS DR7; Azabaijan et al. 2009), providing more extended coverage beyond r_{200}.

This paper is structured as follows. Section 2 details the simulations used and presents information on the simulated clusters. Section 3 describes the NFPS and SDSS data in more detail. Section 4 describes the star formation models employed and compares the resulting trends in galaxy colours with observations. The predicted line strengths are compared to observations in Section 5. We discuss the implications of our results in Section 6 and summarize and conclude in Section 7. Further discussions of merger prescriptions and simple star formation models are available in Appendix A.

2 N-BODY SIMULATIONS AND HALO ORBITS

2.1 Methods

The simulation data consists of four rich clusters generated using the publicly available parallel TREE-PM code GADGET-2 (Springel 2005). Cluster candidates were identified from a low-resolution initial simulation using 256^3 particles in a cube of side length $512h^{-1}$ Mpc. Λ cold dark matter cosmological parameters $\Omega_\Lambda = 0.72$, $\Omega_m = 0.28$, $h = 0.72$ and $\sigma_8 = 0.8$ were adopted, consistent with *Wilkinson Microwave Anisotropy Probe* 7-yr results (Komatsu et al. 2011). Four candidate clusters were chosen for a higher resolution 'zoom' re-simulation (Katz & White 1993; Navarro & White 1994; Power et al. 2003), producing 150 approximately equally spaced snapshots from $z = 3$ to $z = 0$. A fifth candidate was excluded due to a complex, late-time merger, which is atypical of cluster growth histories. In brief, only particles passing near the central overdensity in each simulation are fully sampled. Particles which remain sufficiently far (in practice, more than about 20 Mpc h^{-1}) are subsampled and given higher masses to provide an accurate tidal field, with four levels of refinement up to the full $512h^{-1}$ Mpc side box. Each re-simulation has 12.5 million dark particles, 8.8 million of which are full resolution with a mass of $6.16 \times 10^8\,\mathrm{M}_\odot\,h^{-1}$. The particle mass and minimum gravitational softening length of $1h^{-1}$ kpc are

Table 1. Properties of the four simulated rich clusters and their subhalo populations at $z = 0$.

$M_{\rm vir}$ ($10^{14}{\rm M}_{\odot}/h$)	R_{200} (Mpc/h)	σ_{1D} (km s^{-1})	$N_{\rm P}{}^{a}$ (10^{6})	$N_{\rm H}{}^{b}$	$N_{\rm I}{}^{c}$	$N_{\rm B}{}^{d}$
17.90	1.98	1176	2.9	33 567	9328	1000
13.89	1.82	1103	2.3	32 605	6468	1437
9.11	1.58	1073	2.7	30 940	7511	1071
9.82	1.62	945	1.6	32 980	4800	989

[a]Millions of particles within the virial radius of the cluster.
[b]Number of haloes ever tracked, including recovered 'orphan' haloes.
[c]Number of haloes which have ever crossed the virial radius of the cluster.
[d]Number of haloes which crossed the virial radius but are now outside of it.

sufficient to resolve a Milky Way or M31 mass halo with at least 1000 particles and achieve a resolution limit of 30 particles per halo for haloes close to the total mass of a dwarf galaxy like the Large Magellanic Cloud.

The masses and other physical properties of each cluster at $z = 0$ are given in Table 1. Subhalo catalogues at each time step were generated using the AMIGA Halo Finder (Knollmann & Knebe 2009, hereafter AHF). AHF calculates isodensity contours on an adaptive mesh grid and identifies subhaloes as collections of mutually bound particles within unambiguous density contours (i.e. overdensities). The resulting subhalo statistics are given in Table 1. AHF determines halo sizes from upturns in radial density contours, using an iterative process to remove unbound particles. We create halo merger trees by linking between consecutive snapshots' subhalo catalogues.

A typical problem with *N*-body simulations of dissipationless dark matter (DM) is the overmerging of low-mass DM subhaloes as they are tidally disrupted by the cluster. This effect has been shown to be at the least strongly resolution dependent (Moore, Katz & Lake 1996), and mostly likely an artefact of poor resolution (Klypin et al. 1999). A common solution to this 'overmerging' problem, adopted here, is to use the most bound particle(s) to track the orbits of these 'orphan' haloes (Kauffmann et al. 1999; Springel et al. 2001). In our implementation, any halo which is detected in at least one snapshot is tracked through its most bound particle in all subsequent snapshots, even if it is not detected again by AHF. Thus, once a halo is detected at high redshift, it is guaranteed to still be present in the final $z = 0$ snapshot. Although AHF is capable of detecting most of the massive subhaloes in the simulation, the most bound particle tracking technique recovers on average four times as many haloes as in the original halo AHF catalogue.

Although this method recovers many genuinely independent subhaloes, it can also recover subhaloes that have genuinely merged. Merging is generally suppressed in massive clusters, since the dynamical friction time-scale is long enough that satellites can survive for billions of years (Tormen, Diaferio & Syer 1998), unlike in lower mass clusters (Tormen 1997). However, merging may not be suppressed in the field prior to infall and may even be enhanced in groups; thus, some of the 'overmerged' haloes that were 'unmerged' by this method may indeed have been genuine mergers prior to cluster infall. Semi-analytical models typically employ prescriptions for dynamical friction and merging to identify such unresolved potential mergers. Our simulations can adequately resolve dynamical friction but are limited in identifying substructure in large overdensities. Potential 'merger candidates' are identified as those orphan subhaloes at less than 75 kpc distance from a more massive parent halo and with a low binding ratio ($v/v_{\rm escape} < 0.1$) at the final time step. While these cuts are somewhat arbitrary and are likely an overestimate of the true number of merged haloes, since some satellites could be at similar distances without having yet been merged, the final consequence of including or excluding these candidate mergers on our results is generally small. We opt to exclude 'candidate merger' subhaloes from our analysis by default. A more detailed comparison of simplistic models with and without this merging prescription is presented in Appendix A.

Besides tracking overmerged haloes, we use the most bound particles to fill in 'gaps' in each halo's orbital history, e.g. for haloes detected in the 8th and 10th snapshot but not the 9th, which can occur if haloes briefly cross dense regions at pericentre, for example.

In this paper, we will typically define 'infall' to occur when the subhalo crosses the virial radius r_{200}, defined to be the radius within which the mean density is 200 times the critical density, or in some models at a smaller fraction of r_{200}. We track r_{200} across all redshifts, so the value evolves and is not fixed to r_{200} at z = 0. The mean cluster density thus drops by a factor of about 3 from z = 1 to the present. The look-back time at the first r_{200}-crossing is noted as $t_{r_{200}}$. The orbits allow us to also define the look-back time to first pericentre passage. For the rich clusters studied here, we find that, for recent infalls, the typically time between infall and pericentre is close to 1 Gyr.

In principle, pericentre can occur anywhere within r_{200}; in practice, few haloes pass closer than $0.1r_{200}$. The median pericentre is $0.4r_{200}$ with no dependence on $t_{\rm infall}$ except at $z \lesssim 0.1$, where it begins to dip to $0.3r_{200}$.

In addition to tracking subhalo positions and velocities after infall, bound particles are used to compute velocity dispersions for each subhalo. Subhaloes are assigned a *maximum* velocity dispersion $\sigma_{\rm max}$ corresponding to the velocity dispersion at the time when the subhalo had the largest mass (and in turn had the largest amount of bound particles) prior to infall within r_{200}. This is based on the assumption that a subhalo will not grow significantly after infall, which is expected to be true. In the real Universe, we might expect the galaxy's baryonic component, which has dissipated and become more tightly bound, to be much less sensitive to tidal disruption than a dissipationless DM halo. Thus, the maximum pre-infall halo velocity dispersion serves as a proxy for the (post-infall) stellar velocity dispersion (Conroy, Wechsler & Kravtsov 2006), which in turn is the primary driver of the stellar populations (see Section 4 below).

The simulations allow us to mimic observational samples by viewing the subhaloes positions and velocities in projection. In all plots of projected quantities, we use the three axial projections of each cluster and appropriate line-of-sight velocities and velocity dispersions to average over projection effects and improve galaxy statistics. We denote the projected radius on the sky as R, to distinguish it from the 3D radius r. We also apply cuts in velocity-space, including all subhaloes with velocity cz within $\pm 3\sigma_{\rm cl}$ of the cluster's mean $\overline{cz}$. Thus, in the plots shown in projection, about 17 per cent of the plotted subhaloes have $R < r_{200}$ although in 3D they are outside the virial radius ($r > r_{200}$). This fraction can vary from 12–20 per cent with velocity dispersion or infall-time related cuts, which we will apply when populating haloes with galaxies in Section 4. For a more detailed discussion of contamination due to projection, see Mamon, Biviano & Murante (2010).

2.2 Results

We now examine cluster-centric trends of the two key subhalo properties to be passed to our galaxy evolution code in Section 4: subhalo

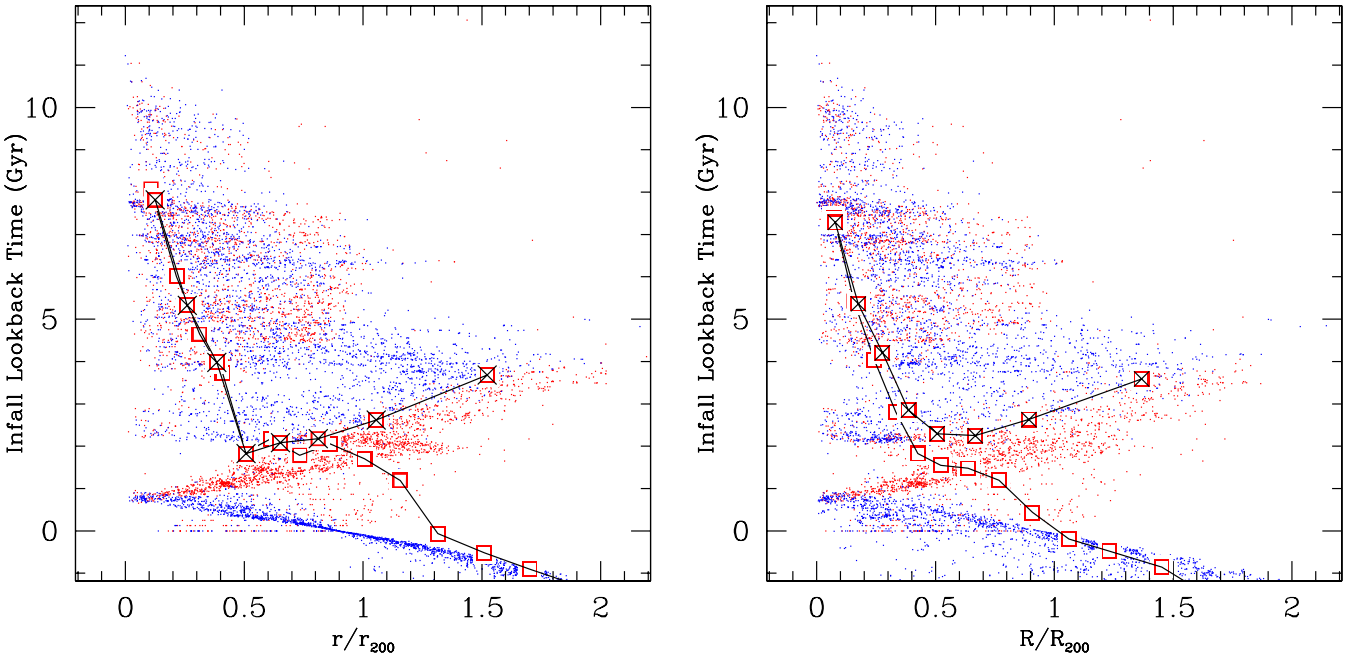

Figure 1. Look-back time at infall (t_{r200}) for subhaloes as a function of radius, in three dimensions (left-hand panel) and in projection (right-hand panel). Haloes are colour coded on whether they are approaching (blue) or receding from (red) the cluster. Haloes that have not fallen in yet are given a naive estimate of their eventual infall time assuming no changes in their current radial velocity and the size of the cluster. Empty squares show the median infall times for all haloes; squares with an x inside show median infall times for only those haloes that have fallen in ($t_{r200} > 0$).

velocity dispersion $\sigma_{\rm max}$ and infall/pericentre time. In our models, these two quantities will determine the star formation history (SFH) of the galaxy stellar populations.

Fig. 1 shows the distribution of subhalo infall times past r_{200} (i.e. time since first crossing of r_{200}) as a function of both projected and real distance to the centre of each cluster. We define accreted haloes as those that have crossed r_{200} of the cluster at least once. Most recently accreted haloes (<2 Gyr) are clustered around the same position for any given infall time, likely because most haloes have mostly radial orbits and thus have similar infall histories. The majority of haloes with intermediate infall times (2–4 Gyr) are at large radii, even outside the virial radius of the cluster and thus form a 'backsplash' population of galaxies that fell into and then back out of the cluster. Few backsplash galaxies remain so longer than 6 Gyr; such old accreted haloes are concentrated near the centre of the cluster. This virialized population of subhaloes outnumbers the very recent infalls within $0.25r_{200}$. At $0.5r_{200}$, the median infall time of a subhalo is barely 2 Gyr.

When considering only accreted haloes, the backsplash population dominates at large radii ($>0.5r_{200}$) and the median infall time increases once again. However, when considering all haloes and not just accreted haloes, the median infall time continues to decrease past r_{200}, simply because the population outside r_{200} is dominated by haloes about to fall in for the first time, rather than haloes exiting the cluster after reaching pericentre. These soon-to-be-accreted haloes can be assigned zero or negative infall times based on estimates for their inevitable infall time on to the cluster (Fig. 1), where a negative median infall time in a particular bin indicates that more than half of the haloes have yet to fall in. The tight linear relation between these estimated infall times and r/r_{200} suggests that most field galaxies within r_{200} are falling in to the cluster on nearly direct radial orbits. As a result and despite the scatter in pericentres, it is clear in 3D that the accreted halo population can be separated by radial velocity up to an infall time of 2–3 Gyr, where these recently accreted haloes begin to reach apocentre. Haloes with $t_{r_{200}} > 4$ Gyr are almost all part of the virialized population, since few are backsplash galaxies and there is a roughly even split between approaching and receding galaxies.

The trends identified in 3D are, of course, less evident in projection. However, the clear distinction between approaching and receding haloes remains. Similarly, there are two triangularly shaped 'holes' in the projected phase space, with virtually no haloes having infall times between 1 and 2 Gyr within $0.5R_{200}$ and very few backsplash haloes with $t_{r200} < 2$ Gyr. If there is a strong environmental impact on infalling galaxies, there should be two distinct populations beyond R_{200} – currently infalling haloes hosting field galaxies and a smaller backsplash population hosting quenched galaxies. Within R_{200}, the distinction is less clear – haloes have a variety of infall times, and some are simply within R_{200} in projection but have yet to cross r_{200}. These projection effects serve to lower the median infall time. As we will demonstrate in Section 4.3, the trends identified in infall time can be mapped on to a stellar population age for haloes hosting galaxies undergoing infall-based quenching, which is particularly appropriate for discs. In particular, the sharp drop in median infall time between 0.8 and 1 R_{200} will cause a similarly large change in optical colours of galaxies for models employing abrupt quenching (AQ) on infall.

These trends are also mass dependent, as will be demonstrated shortly. At any given radius, the median infall time is larger for massive haloes, and so the trends shown in Fig. 1 become smoother when smaller haloes (which are unlikely to host massive galaxies) are excluded. The small population of haloes close to the cluster centre but with very small infall times ($r < r_{200}$, $t_{\rm infall} < 0.3$ Gyr) are mostly spurious numerical artefacts, which tend to be very low mass haloes at the resolution limit and not real galaxies. Finally, it should be noted that haloes can also fall in to a group before reaching the cluster. Groups of multiple haloes can then fall in to the cluster nearly simultaneously, and a few such groups are visible

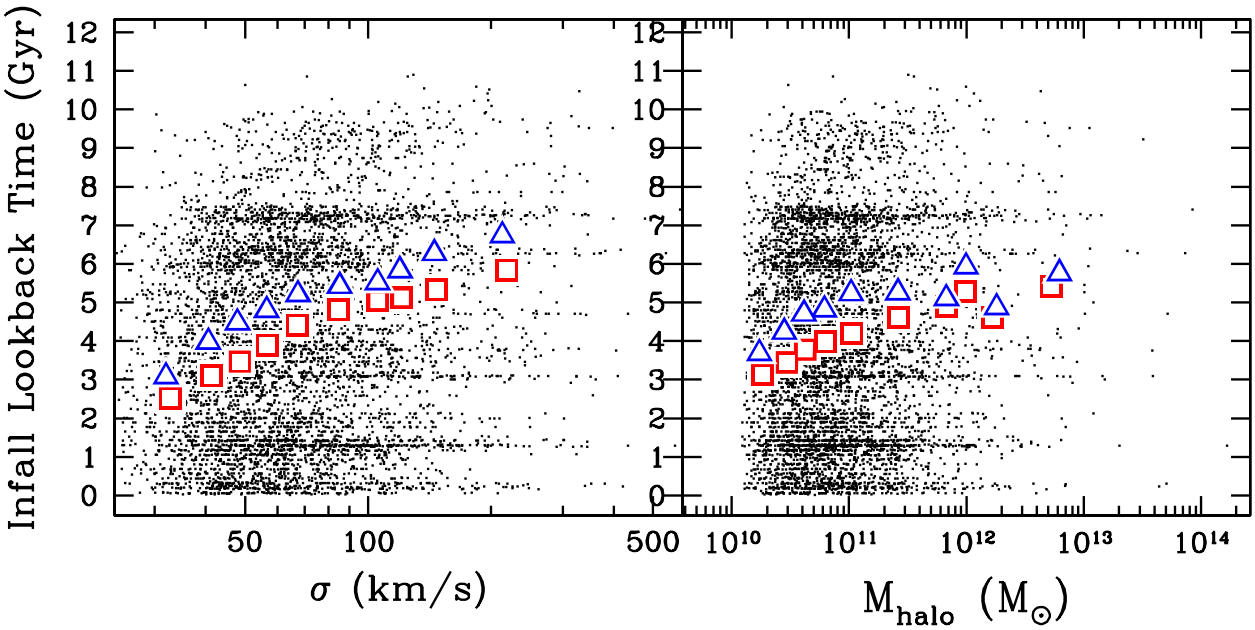

Figure 2. The median look-back times at infall of subhaloes as a function of pre-infall velocity dispersion (left-hand panel) and pre-infall mass (right-hand panel). The squares show the median infall times of all subhaloes which have fallen in. The triangles show median infall times only for those subhaloes which are unlikely to have merged. Haloes with higher velocity dispersions are more likely to have fallen in longer ago, whereas this trend is weak for more massive haloes.

as bands of haloes at very similar infall times in Fig. 1. This effect is partly diluted by the superposition of data from four different clusters.

Although there is considerable scatter, subhalo infall times are also correlated with the velocity dispersion and mass of the halo (Fig. 2). The median infall time for dwarf haloes ($\sigma < 50$ km s^{-1}) is 2–3 Gyr, while most massive subhaloes ($\sigma > 150$ km s^{-1}) fell in at least 2 Gyr ago, with a median of 6 Gyr. This can be interpreted as a consequence of the spatial correlation/clustering of overdensities in the early Universe, such that the largest overdensity collapsed into the cluster itself, while nearby overdensities formed massive subhaloes which fell in at early times. The trend with halo mass is quite weak, especially above 2×10^{11}M$_\odot$, and it is also sensitive to prescriptions for merging and pre-processing. The trend with velocity dispersion is robust, as it is a natural consequence of the fact that haloes with large infall look-back times are more likely to have formed at higher redshift, and thus have higher densities and dispersions at a fixed mass.

The consequences of this correlation on galaxy formation models are that even a purely environmentally quenched model would predict a non-zero slope in the colour–magnitude relation, since higher dispersion (and more luminous) galaxies would have fallen in earlier and hence be redder on average. Opposing trends have been identified in the literature (e.g. fig. 7 of De Lucia et al. 2012, which suggests that the most massive galaxies have fallen in more recently on average). We find that the direction of the weak mass trends in our simulations can be reversed by incorporating pre-processing and by allowing for more mergers, as in De Lucia et al. (2012), whereas the stronger trends with halo dispersion remain robust.

In addition to the mass trend, there is a weak but non-zero trend in the median velocity dispersions of haloes as a function of cluster-centric distance (Fig. 3), even in projection. This can be viewed as a combination of the infall time versus position (Fig. 1) and infall time versus mass relation (Fig. 2), which essentially causes mass segregation of subhaloes. However, the trend appears to be strongest for low-mass haloes and is weaker for haloes likely to host massive galaxies (which we identify using a typical model from Section 4).

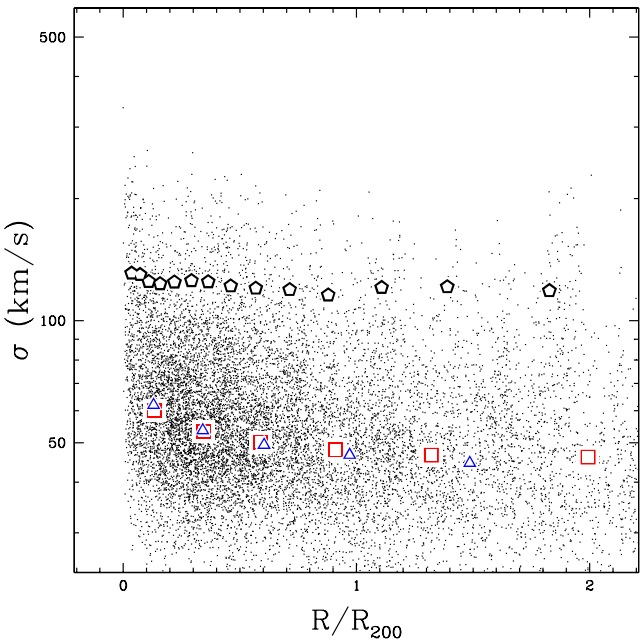

Figure 3. Velocity dispersions of haloes as a function of projected separation from the cluster centre. Red squares show the median velocity dispersion at various radii; blue triangles exclude orphan haloes which are likely to have merged, as in Fig. 2. Black pentagons show medians only for haloes likely to contain bright galaxies. High dispersion subhaloes tend to be found near the cluster centre, where the median velocity dispersion is ∼20 km s^{-1} greater than in the field. This trend is not as strong for massive haloes likely to host bright galaxies.

3 DATA

We constrain our models using data for giant galaxies in clusters from the NFPS (Smith et al. 2004) of ∼3000 galaxies in 94 nearby rich clusters. Colours for 750 giant ($M_R < -20.25$) galaxies in eight rich clusters are taken from Hudson et al. (2010). This subsample has no colour selection and includes red and blue galaxies. It provides (total) galaxy colours in $B - R$ as well as colours in the same filters for the bulge and disc components separately. Spectroscopic data, in the form of central absorption line indices, are from Nelan et al. (2005). The NFPS spectra are too noisy to obtain ages and metallicities for individual galaxies, but the trends as a function of internal velocity dispersion σ and projected distance from the cluster centres are well determined (Smith et al. 2006).

In addition to NFPS, we also employ a larger data set from SDSS, which remains complete to nearly arbitrary distances from the cluster core. We combine the bulge-disc decompositions of Simard et al. (2011) with a catalogue of 625 brightest group and clusters galaxies from von der Linden et al. (2007), which is based on the catalogue of Miller et al. (2005). This provides total, bulge and disc colours in $g - r$ for all galaxies in each group, as well as distances relative to the cluster centre (typically the brightest cluster galaxy). Likely background galaxies with projected velocities $v > 2\sigma_{3D}$ ($v > 3.46\sigma_{1D}$) are excluded, where σ_{1D} is the measured (projected) velocity dispersion of the cluster, and σ_{3D} the estimated 3D dispersion. To compare to the simulated cluster sample, we select only the 28 clusters with $\sigma_{1D} > 800\,\mathrm{km\,s^{-1}}$. Within a distance of $4R_{200}$, there are about 5000 galaxies in this sample. This data set will be described further in an upcoming paper (Oman et al., in preparation).

The mild trend predicted for the median masses of subhaloes to decrease with radius (Fig. 3) appears to be in conflict with recent observations of satellite galaxies of luminous red galaxy (LRG)-selected groups from SDSS (Budzynski et al. 2012), in which faint galaxies are prevalent near group centres. The cause of this discrepancy is not known, but is suggestive of a differences in mass segregation of subhaloes in the lower mass haloes studied in Budzynski et al. (2012), compared to the more massive and lower redshift subhaloes studied here. Our own NFPS and SDSS data show no radial trend in median galaxy magnitude within massive clusters.

4 STAR FORMATION MODELS AND COLOURS

We will now use the halo orbits of Section 2.2 as input to simple star formation models in which environmental 'triggers' quench star formation – more specifically, cluster-centric triggers such as infall past r_{200} or reaching pericentre. This quenching can either be slow (e.g. causing an exponential decay in the SFR), or abrupt. At first, we will only consider models where quenching occurs within the cluster (i.e. after infall on to the cluster halo); later, we will incorporate pre-processing by allowing quenching by smaller group-sized haloes.

4.1 Galaxy catalogues and stellar masses

To generate mock galaxy catalogues from the DM only simulation, each subhalo is assumed to host a single galaxy. Stellar masses are assigned to galaxies based on their DM halo's velocity dispersion. The favoured model maps dark matter halo (DM) dispersions to stellar ($\star$) dispersions using the relation between maximum halo circular velocity and circular velocity at 10 kpc from Trujillo-Gomez et al. (2011): $\log(\sigma_\star) = -0.236 \times (\log(\sigma_{\rm DM}))^2 + 1.734 \times \log(\sigma_{\rm DM}) - 0.5723$ (this fits the Einasto profile/Bolshoi lines of fig. 3 of Trujillo-Gomez et al. (2011)). In effect, we assume that the ratio $\sigma_{\rm DM}/\sigma_\star = v_{\rm circ,max}/v_{\rm circ,10kpc}$. This maps the excessively large dispersions of massive haloes into more appropriate stellar dispersions. Stellar masses are then assigned by selecting SDSS early-type galaxies (Simard et al. 2011) using the criteria outlined in Taranu, Dubinski & Yee (2013, section 4.1), yielding the following best-fitting relation: $\log(M_\star) = 3.498 \times \log(\sigma_\star) + 3.225$. In summary, for each halo, we convert $\sigma_{\rm DM}$ to $\sigma_\star$, and then $\sigma_\star$ to $M_\star$, preserving rank ordering. We have also tested an alternative prescription whereby halo velocity dispersions are converted to stellar masses from the best-fitting σ–$R_{\rm eff}$ relation for Coma galaxies from Allanson et al. (2009), more representative of rich cluster members. While this yields a slightly higher abundance of bright galaxies, the differences in typical galaxy colours between the two prescriptions (0.01–0.02 in B–R) are smaller than typical observational errors on median colours (0.03–0.04). Lacking any reason to favour this prediction, we employ the SDSS-based prescription in all cases.

After assigning stellar masses, the SFH of each galaxy determines stellar mass-to-light ratios and magnitudes. The final simulated galaxy catalogue contains only galaxies brighter than the observational limits of the data, i.e. $M_R < -20.25$, or a roughly equivalent cut of $M_r < -20.01$. These magnitude cuts typically exclude haloes with dispersions below $\gtrsim$100 km s^{-1}, or $M_{\rm stellar} \gtrsim 10^{10}\mathrm{M}_\odot$ – thus, the catalogue only contains galaxies in haloes which are well above the simulation's resolution limit. The subhaloes that host these galaxies have masses $M_{\rm halo} \gtrsim 10^{11}\mathrm{M}_\odot$. The median and mean stellar masses of galaxies in the sample are $M_{\rm stellar} \sim 2.5 \times 10^{10}\mathrm{M}_\odot$ and $\sim 5 \times 10^{10}\mathrm{M}_\odot$, respectively.

4.2 Median colours as a function of cluster-centric radius

Throughout this section, the primary statistic used to compare models and data will be the median colour in bins of cluster-centric radius. The median has the advantage that it is robust to outliers.

Although we will discuss qualitatively the colour distributions produced by different models, we are reluctant to draw strong conclusions based on the full shape of the $B - R$ colour distribution for two reasons. First, the observational uncertainties on individual galaxy colours (∼0.1 mag for discs; Hudson et al. 2010) are not included in our models; these would scatter the intrinsic distribution and preclude the rejection of any model based on colour bimodality. Secondly, we will show that our default model for the unquenched blue cloud is simple: a simple exponential time-scale prior to infall and a second one following quenching for recently quenched satellites. To realistically model the spread in the blue population, one would likely need to incorporate scatter in the star formation histories and metallicities, none of which are well constrained by the data. For these reasons, the median colours are expected to be a more robust statistic than the full distributions of $B - R$ colours.

The same argument applies to blue fractions. Unlike the case for, say, $u - r$ colours (Balogh et al. 2004), in $B - R$, Hudson et al. (2010) show that there is no well-defined bimodality in the observed colours of cluster galaxies, not in the least because there are fewer blue galaxies than in the field. It is therefore difficult to determine where to separate blue and red. Moreover, given that the blue and red populations are close and overlapping, correct treatment of the scatter (observational and in the models) is essential for obtaining the correct fractions.

4.3 Single-component toy models

We first explore two simple toy models designed to test the influence of cluster-centric environment. These are 'single component' models in which the entire stellar population of the galaxy is described by a single SFH. Although such models are not expected to be good matches for cluster galaxies on their own, we can test if they are appropriate fits to the distinct bulge and disc components.

4.3.1 The AHS star formation models

We will use the Allanson et al. (2009, hereafter AHS) SFH models as baselines for our single-component models. The AHS models parametrized the SFH in terms of simple functional forms (e.g. single burst, exponential, constant SF followed by 'AQ', etc.) and then adjusted the parameters of the model in order to reproduce both the median and the scatter in the global colours and central spectroscopic line indices of NFPS red-sequence galaxies. Several studies (Graves et al. 2009; Smith et al. 2009a) have shown that stellar populations are more tightly linked to the velocity dispersion than to the stellar mass, so a priori, one expects a correlation between mean stellar age and the stellar velocity dispersion. In the AHS models, the central stellar velocity dispersion determines (1) an age-related parameter, such as a Single/Simple Stellar Population (hereafter SSP) age or a quenching time, (2) the metallicity and (3) the α-enhancement. Random scatter is added to each of these parameters to generate a galaxy population with a distribution of ages, metallicities and α-enhancements. For each simulated galaxy, the stellar population parameters are used to generate simulated colours and absorption line-strength indices calculated by convolving SSP model SEDs (Maraston 1998, 2005) and Lick-index absorption line strengths (Thomas, Maraston & Bender 2003) with a given SFH in order to reproduce the line indices of red-sequence cluster galaxies from Nelan et al. (2005) and Smith, Lucey & Hudson (2007). Having done so, AHS find reasonable agreement with galaxy colours as well, with the caveat that $B - R$ colours are too red by about 0.1 mag, a common problem in stellar population models and one which will be addressed shortly. Furthermore, the AHS models include synthetic total magnitudes, allowing us to select samples in the same way as the real NFPS data. Thus, by construction the AHS models should match the observed red-sequence stellar population observables, with the caveat that the SSP colours are likely to be too red (Maraston et al. 2009). Finally, in all cases we assume a universal Kroupa (2001) stellar initial mass function (IMF).

4.3.2 Internal quenching versus quenching on cluster infall

To test the impact of environment on star formation in cluster galaxies, we employ two simple models – one with an indirect relation between environment and star formation, and one with a more direct impact. The first ('null hypothesis') model is one in which the cluster environment has no direct effect: we assume that the SFH depends *only* on internal properties of the subhalo (specifically the velocity dispersion of the subhalo), and not on infall into the cluster. SFR are modelled either as declining until a specified time $t_{\rm AQ}$ or as a single instantaneous burst (SSP). The α-enhancement and metallicities are assigned through a lookup table of similar galaxies in the AHS mock catalogues. This yields a red sequence in which stellar population age, and hence galaxy colour, depends only on the *internal* properties and not explicitly on position in the cluster. Nonetheless, colours in this model have a weak and indirect dependence on cluster-centric radius due to the correlation between subhalo velocity dispersion and cluster-centric radius noted in Section 2. We will explore this trend further in Section 4.4.

In the second simple model, the galaxy's internal velocity dispersion has no effect on its age and metallicity. Instead, the quenching time is set to the look-back time at which it fell into the halo, i.e. the time at which it first crossed r_{200}. Metallicities and α-enhancements are set to solar with small (<0.05 dex) scatter. We model the SFR as exponentially declining – prior to infall, with some pre-infall e-folding time $\tau_{\rm pre}$, and subsequently with a post-infall e-folding time $\tau_{\rm post}$. We have also considered models where quenching begins at pericentre, where environmental effects are strongest. In practice, most subhaloes of the cluster take 0.5–1 Gyr to reach pericentre from r_{200}, and so quenching at pericentre is quite similar to (but more physically motivated than) a fixed delay time of about 1 Gyr.

Environmental quenching as in the infall-based model produces a wider range of galaxy colours and a steeper dependence of colour on cluster-centric radius. Galaxies that have recently (or never) fallen in have the bluest colours, dominating the outskirts of the cluster. In the core of the cluster, the time since infall spans a range from several hundred Myr for the most recently accreted haloes still on their first orbit around the cluster core, to many Gyr for older, virialized haloes. Hence, the overall colour gradient is a function of the relationship between infall time and position (Fig. 1) modulated by the dependence of colour on infall time. The former relation is almost entirely determined by cosmology, while the latter is dependent entirely on our choice of star formation model.

The simplest models one can construct are either entirely internally quenched, or entirely environmentally quenched. A naive choice for the parameter $\tau_{\rm pre}$ of infinity results in a constant SFR; however, this produces excessively blue colours for field galaxies. A similar naive choice of $\tau_{\rm post} = 0$ produces excessively large gradients in colours. Finally, the internally quenched SSP model produces virtually no gradient. These trends are examined in greater detail in Appendix A. We now turn to more realistic bulge/disc models using multiple components based on these simple toy models.

4.4 Bulge plus disc models

4.4.1 Environmental dependence of bulges and discs

The $B - R$ colours of bulge and disc components of giant galaxies in clusters were studied by Hudson et al. (2010). They found that bulge colours were redder than discs (as expected) but that bulge colours were independent of cluster-centric radius. In contrast, the colours of disc galaxies depend significantly on cluster-centric radius and drive the weaker gradients observed for global colours. The lack of radial dependence of the bulge colours is therefore similar to the predictions of the 'internally quenched' toy model above, whereas the radial dependence of the disc colours is similar to the infall-quenched toy model. This suggests that we build a composite bulge/disc model in which only the discs are affected by environment.

In the NFPS data, the bulge-to-disc ratio varies along the red sequence, with higher mass systems being more bulge-dominated. Indeed AHS showed that the bulge-to-total light ratio (B/T) was tightly correlated with central velocity dispersion (see their fig. A1). We use their empirical relation to determine B/T at a given velocity dispersion, σ: $(B/T)_R = 0.5 \times \log(\sigma_\star) - 0.44$. Typical galaxies with velocity dispersions of 100 km s^{-1} have 54 per cent of their light in the bulge, while the most massive galaxies are over 80 per cent bulge dominated.

4.4.2 Bulge model

Having assigned bulge fractions, bulge ages are then generated as for the 'internally quenched' toy model described above. The bulge metallicity is determined by drawing a random galaxy from the AHS catalogue with a similar stellar dispersion (±0.1 dex). The AHS catalogue provides a total metallicity, α-enhancement and model-dependent age for the galaxy, derived from fits to line index strengths (not colours) – we use this same age for the bulge, and give the bulge sufficiently large metallicity and α-enhancement to match the AHS value. In practice, almost all bulges have super-solar metallicity and are increasingly metal rich at larger velocity dispersions. By contrast, discs are assumed to have solar metallicity with small (<0.05 dex) scatter and no α-enhancement. Since the total metallicity is a mass-weighted average of the disc and bulge metallicities, we adjust the bulge metallicity to reproduce the desired total metallicity (which typically increases the bulge metallicity by 0.05–0.1 dex. The bulge α-enhancement is adjusted in a similar fashion.

For the most part, bulge colours are constant with cluster-centric radius in both the models and data, as shown in Fig. 4. The main exception is that the SDSS galaxies show slightly bluer bulge colours in the inner regions of the cluster. This could be connected with the fact that bulge fractions in SDSS r-band are both lower (about 47 per cent on average versus 57 per cent in NFPS) and slightly higher in the cluster core (53 per cent) than in the outskirts (44 per cent), a trend which is not present in NFPS. This trend could be real or entirely systematic – the SDSS data covers a much larger redshift range, and was generally taken with shorter exposures and worse seeing on a smaller telescope than NFPS, so the existence of this relatively small trend is not especially worrisome.

Of greater concern is that the simulated bulge colours are too red by at about 0.15 mag in $B - R$ and 0.1 mag in $g - r$. This is a well-known problem in stellar population modelling and is detailed by, amongst others, Maraston et al. (2009) (whose stellar population models are used here, uncorrected). The AHS models themselves have a similar offset in bulge colours, which can only be partially corrected by solutions such as modelling the effect of α-enhancement (AHS). However, it should be noted that the ages and metallicities in the AHS models do reproduce line-strength indices by construction and as intended, likely because the effects of α-enhancement are better modelled for line-strength indices. Thus, it is likely that any mismatch in bulge and/or total colours is due to a weakness in stellar population model predictions of colours (but not line-strength indices).

Unfortunately, no current stellar population models entirely correct for this issue. Maraston et al. (2009) suggest including a small fraction of very metal poor and old stars; however, little direct evidence exists for such a population, and a very large fraction (about 10 per cent) is required to entirely explain the offset. α-enhancements are not yet accurately or self-consistently modelled. The remaining option is to apply an artificial shift to the colours directly, or to artificially lower bulge metallicity and age. The '−C' (corrected) model in Fig. 4 applies a fixed −0.u14 shift in $B - R$. Alternatively, lowering the metallicity by 0.3 dex and age by 1.5 Gyr accomplishes the same task – however, this is not a suitable physical solution, since these ages and metallicities are inconsistent with ages and metallicities derived from absorption line strengths. Thus, for the remainder of the paper, we will apply this fixed shift of −0.14 in $B - R$ and −0.095 in $g - r$, and models using this shift will be postfixed with '−C'.

4.4.3 Disc quenching model

The above prescriptions fix the stellar populations of the bulge and also the metallicity and α-enhancement of the disc. This leaves only the SFH of the disc to be modelled. We first consider disc colours

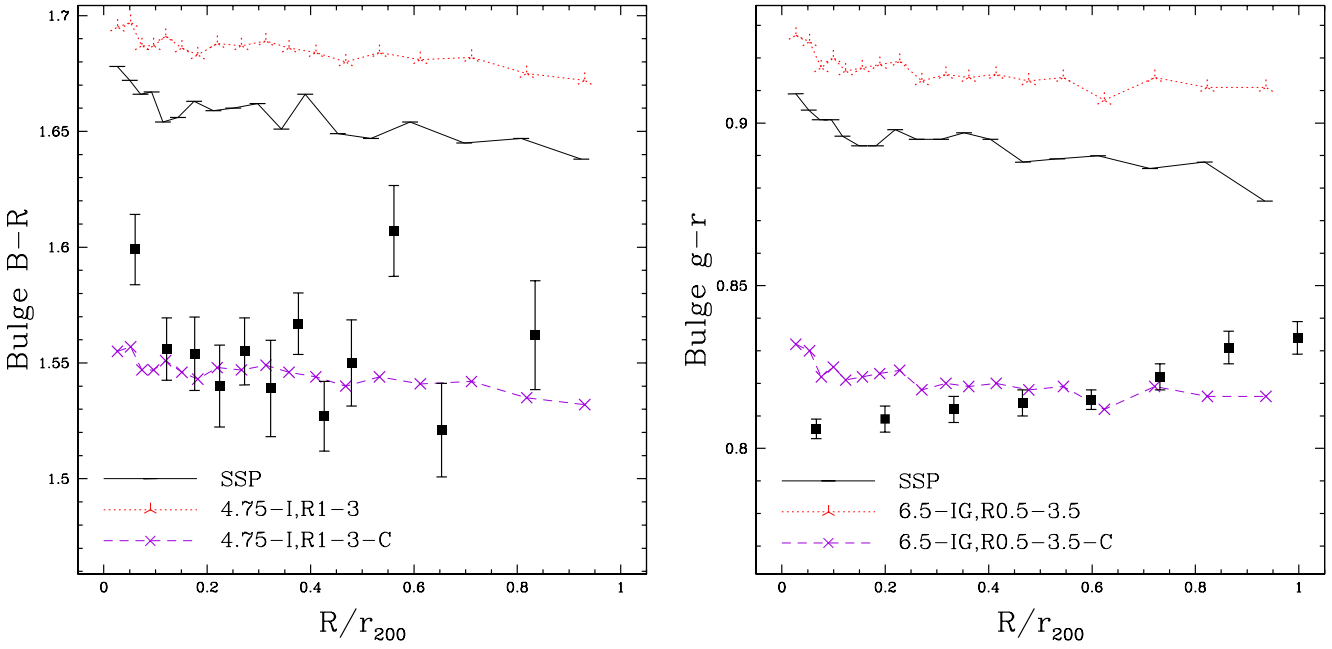

Figure 4. Simulated median bulge $B - R$ and $g - r$ colours for cluster galaxies, compared to data from NFPS $B - R$ colours (left) and SDSS $g - r$ colours (right). The colour of the bulge component is shown for an SSP and a typical bulge + disc model; however, it is flat and essentially independent of the disc model, and remains so well beyond R_{200}. However, simulated bulge colours are too red, a common problem in stellar population models of massive early-type galaxies. The corrected model ('−C') is shifted by −0.14 mag (bluer) to better match the observed trend, as discussed in the text. Galaxies with small bulge fractions ($B/T_R < 0.2$) are excluded from this figure.

in the field, where there is assumed to be no quenching. For field discs, we adopt an exponentially decaying SFH and constrain the *e*-folding time-scale so that the colours match the median colour of discs in the field: $B - R = 1.25 \pm 0.05$ (Hudson et al. 2010). This is in reasonable agreement with the colours found by MacArthur et al. (2004) for discs in field spiral galaxies in the same magnitude range as the NFPS sample.

We find that the observed colours can be fitted with a (pre-quenching) exponential time-scale $\tau_{\rm pre} = 4.5$–5 Gyr. $\tau_{\rm pre} = 4.75$ Gyr yields a $B - R$ of about 1.26 in the field. Similarly, the SDSS field $g - r$ colour of about 0.6 can be reproduced with $\tau_{\rm pre} = 6.5$ Gyr. The difference between these two values of $\tau_{\rm pre}$ could again be partly real, or partly systematic differences between bulge-disc decompositions in the two sample, and uncertainties in stellar population models.

In our bulge/disc models, disc quenching will be caused by interaction with the cluster environment. There are two parameters that control the quenching. The first parameter controls how *rapid* the quenching is. In the simplest scenario, star formation is instantly and completely suppressed, as might be expected if the quenching is due to ram-pressure stripping of cold gas. We refer to this as AQ. Alternatively, star formation may be quenched more gradually, as in the 'strangulation' scenario. We model this as a second exponential decay in the SFR. The exponential decay time *after* quenching, $\tau_{\rm post}$, is uncertain and so below we experiment with different values. Note that in this context AQ corresponds to $\tau_{\rm post} = 0$. In practice, AQ is strongly disfavoured by the data, and so non-zero values of $\tau_{\rm post}$ are required.

Two additional parameters control how quenching proceeds. One parameter determines *where* in the cluster quenching first occurs: at r_{200} (I) or at pericentre (P). An additional parameter 'R' determines how far the influence of the cluster stretches as a factor of r_{200}. By default (if not otherwise specified) and in most models this parameter has a value of one – i.e. galaxies are quenched after crossing r_{200}. In some models, however, R can be smaller than 1. In the case of $R = 0.5$, only haloes which cross $0.5r_{200}$ are considered as accreted and hence quenched, so haloes with pericentres at $0.6r_{200}$ would not be quenched.

These three parameters suffice to identify most models. Rather than giving models unique names, we simply refer to them with hyphenated values of these parameters in the format: $\tau_{\rm pre}$-Quenching Location,Radius-$\tau_{\rm post}$. For example, AQ on crossing r_{200} would be ∞-I,R1-0. A more complicated model with $\tau_{\rm pre} = 4$ and $\tau_{\rm post} = 3$, with galaxies quenched after crossing $0.3r_{200}$ would be labelled 4-I,R0.3-3.

Fig. 5 shows the best-fitting models incorporating merging but not pre-processing, for both NFPS and SDSS data. Again, a $\tau_{\rm pre}$ value of 4.75 Gyr fits NFPS data well, while the colours of SDSS galaxies at $R/r_{200} > 2$ are best fitted by a value of 6–6.25 Gyr. Similarly, the best-fitting values of $\tau_{\rm post}$ are 3 Gyr for NFPS and 3.5 Gyr for SDSS. As previously mentioned, it is not known to what extent these offsets are due to systematics in the observations or models. However, we do note that an intermediate model with $\tau_{\rm pre} = 5.5$ Gyr and $\tau_{\rm post} = 3.5$ Gyr needs only small corrections of the order of 0.03 mag in either direction ($+0.04$ in B, -0.02 in g) to reproduce both colours, and such errors are rather small considering known systematics in stellar population modelling and comparing two entirely different samples taken with different filters on different telescopes. For example, an offset of 0.15 in g and 0.02 in $g - r$ exists between a Salpeter IMF, $\tau = 1$Gyr model with Maraston (2005) population models compared to the updated Bruzual & Charlot (2003).

What is clear is that some quenching is required to reproduce the colour trends, in the sense that $\tau_{\rm post}$ is significantly smaller

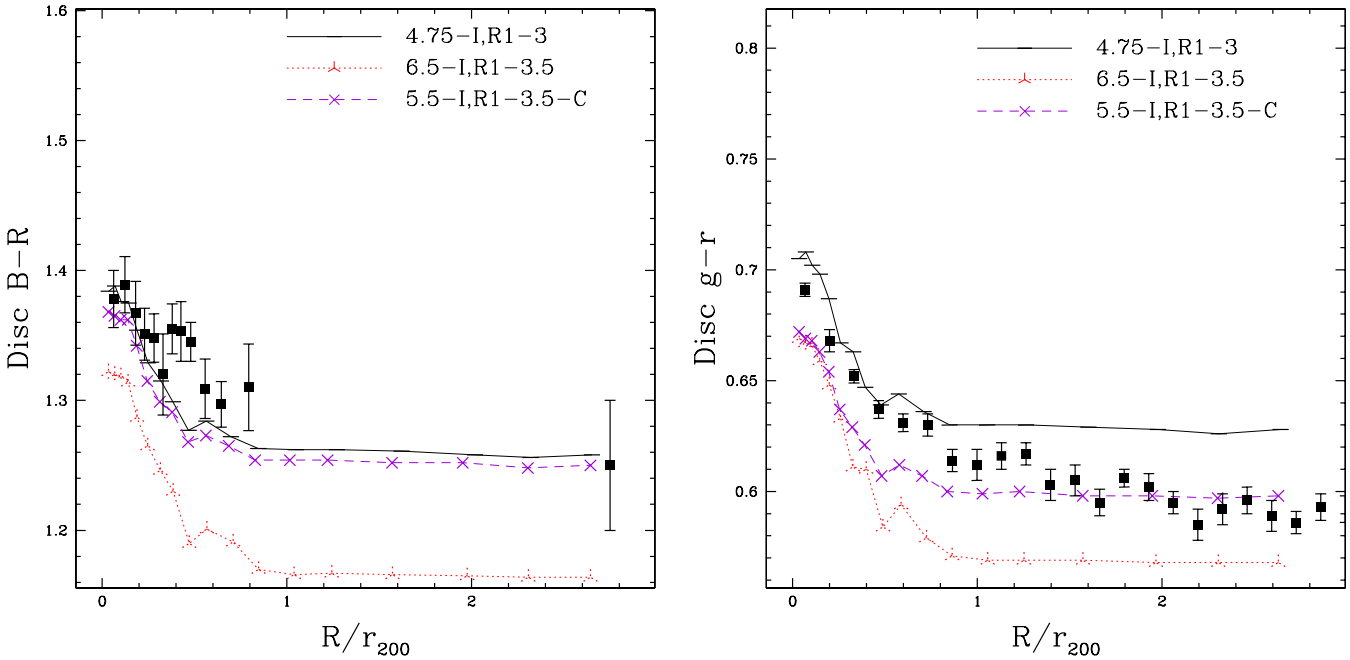

Figure 5. Simulated median disc $B - R$ and $g - r$ colours for cluster galaxies, compared to data from NFPS and SDSS (as in Fig. 4). These models incorporate merging but not pre-processing, with a $\tau_{\rm pre}$ tuned to fit field colours in each sample. The SDSS data prefer larger values of $\tau_{\rm pre}$ and $\tau_{\rm post}$. In both cases, the trend in median colours within $0.5R/r_{200}$ is too steep. The outermost data point for NFPS represents the colours of field galaxies and is not actually a bin at $2.7R/r_{200}$. The '−C' (corrected) model represents an 'average' model, which fits both NFPS and SDSS data with small offsets in the B magnitude of the disc: $+0.04$ in B, and -0.02 in g. Galaxies with large bulge fractions ($B/T_R > 0.8$) are excluded from this figure.

than τ_{pre} – models with $\tau_{post} = \tau_{pre}$ do not produce any colour trend. However, the quenching appears mild on average – τ_{post} is smaller than τ_{pre} by about 40 per cent across most models, but τ_{post} – which is essentially the quenching time-scale – is still quite long, at between 3 and 3.5 Gyr. It is also evident that models without pre-processing produce too steep of a trend in colours, even if the quenching radius is extended to $1.5r_{200}$. Although the median colour at the cluster core is matched, the model colours drop to the field value at about $0.5R_{200}$, whereas observed colours only appear to flatten well beyond R_{200}. This is simply because no galaxies are quenched prior to crossing r_{200}, and the median colours at 0.5–1 R_{200} are still sensitive to projected field galaxies, none of which are quenched in this model. Thus, pre-processing appears necessary to match the observed shallow slope in disc colours, regardless of the value of τ_{pre}.

4.4.4 *Pre-processing: quenching in groups before cluster infall*

Although rich clusters are extreme environments and a likely location for environmental quenching, it is also possible for mechanisms such as stripping and strangulation to occur in less massive clusters and groups prior to infall on to the richest clusters – so-called 'pre-processing'. To implement pre-processing, we allow any haloes of mass greater than $10^{13}M_{\odot}$ to quench infalling satellites. Models incorporating such pre-processing are labelled with a 'G' following τ_{post}, since infall can now occur on to group-sized haloes.

Pre-processing quenches cluster members prior to their infall on to the cluster, increasing their (look-back) infall time, and also quenches field galaxies which have yet to fall in to the cluster. For typical models, 60–65 per cent of cluster members are quenched in a smaller group prior to infall; a slightly higher fraction of projection effects are also quenched. These fractions are larger than the 40–50 per cent found by McGee et al. (2009), but note that the clusters in our sample are also more massive than the most massive of McGee et al. (2009). McGee et al. (2009) also found that pre-processed fractions are larger for more massive clusters.

Pre-processing can occur any time from 0 to 10 Gyr before infall on to the cluster, but median and mean times between pre-processing and infall on to the cluster are 2.5 and 3.5 Gyr, respectively. Thus, pre-processed cluster members are quenched about 3 Gyr earlier than they would have been without pre-processing. Finally, close to half of all galaxies in the simulation have been quenched, so about half of the field has been pre-processed. This change in the fraction of quenched galaxies at all radii – even well outside R_{200} – can be compensated for by increasing τ_{pre}. In practice, SDSS field colours remain virtually unchanged with pre-processing, and only a very minor change from 4.75 to 5 Gyr is needed for the NFPS data.

4.4.5 *Delayed quenching and bimodality*

In a similar study to this one, Wetzel et al. (2013) found good agreement with SDSS observations of specific star formation rates (sSFRs) using models with 'delayed-then-rapid' quenching. The rapid quenching preserves the bimodality in the sSFRs observed by Wetzel, Tinker & Conroy (2012), whereas the delay is necessary to match the overall quenched fraction as a function of environment. Their best-fitting model does not begin quenching until ∼3 Gyr after infall, whereupon quenching is rapid: $\tau_{post} \sim 0.5$–1 Gyr. We implement this by adding a constant delay time to the quenching time. The effect is similar to pericentre-based quenching, but with a longer delay after infall: pericentre occurs after at most ∼1 Gyr. After 3 Gyr, galaxies are typically in the 'backsplash' population (or soon to be virialized).

Fig. 6 compares this 'delayed-then-rapid' quenching model to three best-fitting strangulation models. The two 3 Gyr delay model (labelled with 'D3', since τ_{post} now only applies after this delay is completed) uses $\tau_{post} = 1$, which is towards the high end of the range for massive galaxies considered by Wetzel et al. (2013). As

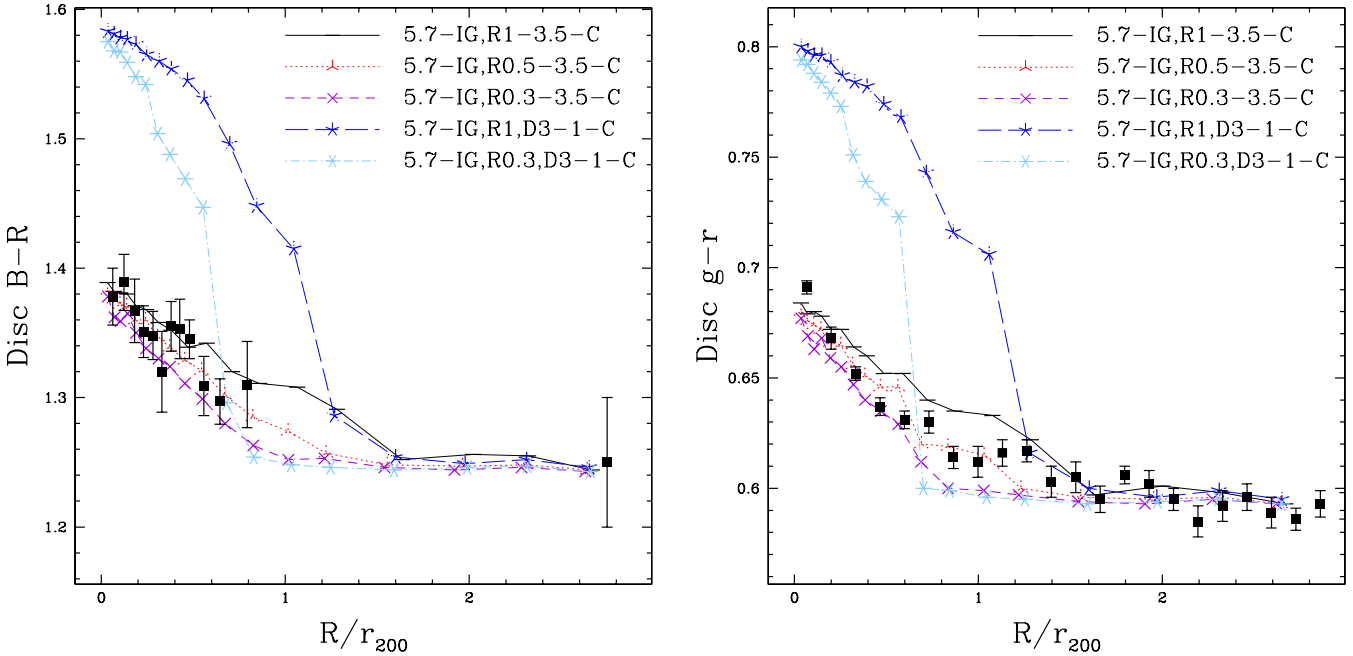

Figure 6. As in Fig. 5, but now for models with pre-processing in groups as well as the main cluster halo. Models are also shown with quenching at radii smaller than r_{200}, or with a delay time D between infall and quenching. The best-fitting model only quenches galaxies falling within $0.5r_{200}$, whereas the 'delayed-then-rapid' quenching model produces excessively red discs near the cluster centre. All disc colours are corrected ('−C') to match median trends, and galaxies with large bulge fractions ($B/T_R > 0.8$) are excluded, as in Fig. 5.

expected, the additional delay keeps more galaxies on the 'blue cloud' compared to a strangulation model with the same $\tau_{\rm post}$. But a weakness of these models is that the mean slope of the $B-R$ versus R/r_{200} is ∼0.25–0.3 mag, whereas the data favour a shallower slope 0.1 ± 0.025 (Hudson et al. 2010). This steep slope is found for *any* model with $\tau_{\rm post} < 1$, whether delayed or not, and the mismatch with observations grows worse with the even smaller values of $\tau_{\rm post}$ favour by Wetzel et al. (2013) for massive galaxies. Moreover, the galaxies closest to the cluster have disc $B-R$ colours that are *redder* than the corrected (and observed) bulge colours. While the disc is younger than the bulge and bluer in pre-correction $B-R$, it is only bluer by a smaller amount than the offset between predicted and observed bulge colours – an uncomfortably thin margin.

One alternative to delayed quenching is simply quenching fewer galaxies by tightening the criteria for quenching. We also tested models quenching only galaxies falling within 0.5 or 0.3 r_{200}. In fact, a quenching radius of 0.5 r_{200} is a better fit to SDSS data and no worse a fit to NFPS data than quenching within r_{200}. This model also lessens the tension in colour bimodality, because at any given time there are fewer galaxies undergoing quenching, and hence fewer intermediate galaxies in the 'green valley'. Applying a similar change to the quenching radius does not, however, improve the delayed-then-rapid quenching models, which maintain the same excessively large slope in disc colours over an even smaller spatial range.

4.5 Consistency check: total colours

We now construct bulge plus disc models and compare them to total colours. In all cases, the bulge component is an SSP; only the disc SFH varies. Such models all produce colour gradients which are mostly compatible with the data (Fig. 7). The slopes are somewhat shallower than observed in all models except the delayed-then-rapid model. Differences between colours in the field and at the centre of the cluster are about 0.12 in $B-R$ (albeit very uncertain due to large errors on field galaxy colours) and 0.065 in $g-r$, but closer to 0.15 in $B-R$ and 0.09 in $g-r$ for the delayed-then-rapid model, and about 0.07 in $B-R$ and 0.04 in $g-r$ for the remaining models. These shallower slopes are a better fit to the shape of both relations, excepting only the innermost, very red bin in both NFPS and SDSS. At very small radii (within $0.2r_{200}$), bulge fractions in SDSS and NFPS are higher than in other spatial bins by 5–10 per cent. In NFPS, this is offset by high bulge fractions in the outermost bin, and so the overall trend in B/T_R is flat. The total colours are redder than the model in exactly these two inner- and outer-most bins, where the model B/T_R is lower than in the data. In SDSS, there is a radially dependent trend in B/T_r, which is not reproduced in the model. B/T_r is also slightly and systematically smaller than B/T_R by another 5–10 per cent, and so the model colours are redder than the data further from the cluster centre.

In conclusion, the total colours are entirely consistent with the disc and bulge colours shown before, with shallower model slopes only due to a weak increase in B/T_r in the data, which is not modelled. Despite the fact that the uncertainties on total colours are smaller, model total colours are relatively less sensitive to the quenching model because they have large bulge fractions but nearly constant bulge colours. Disc colours are a better discriminant of star formation models. This is true not just for the data and models compared here, but for any sample of galaxies with substantial old and red passive components.

4.6 The effect of dust

Galaxy colours are, of course, sensitive to the presence of dust. Driver et al. (2007) find that, on average, bulge+disc galaxies in the field have a some attenuation of B-band light, well described

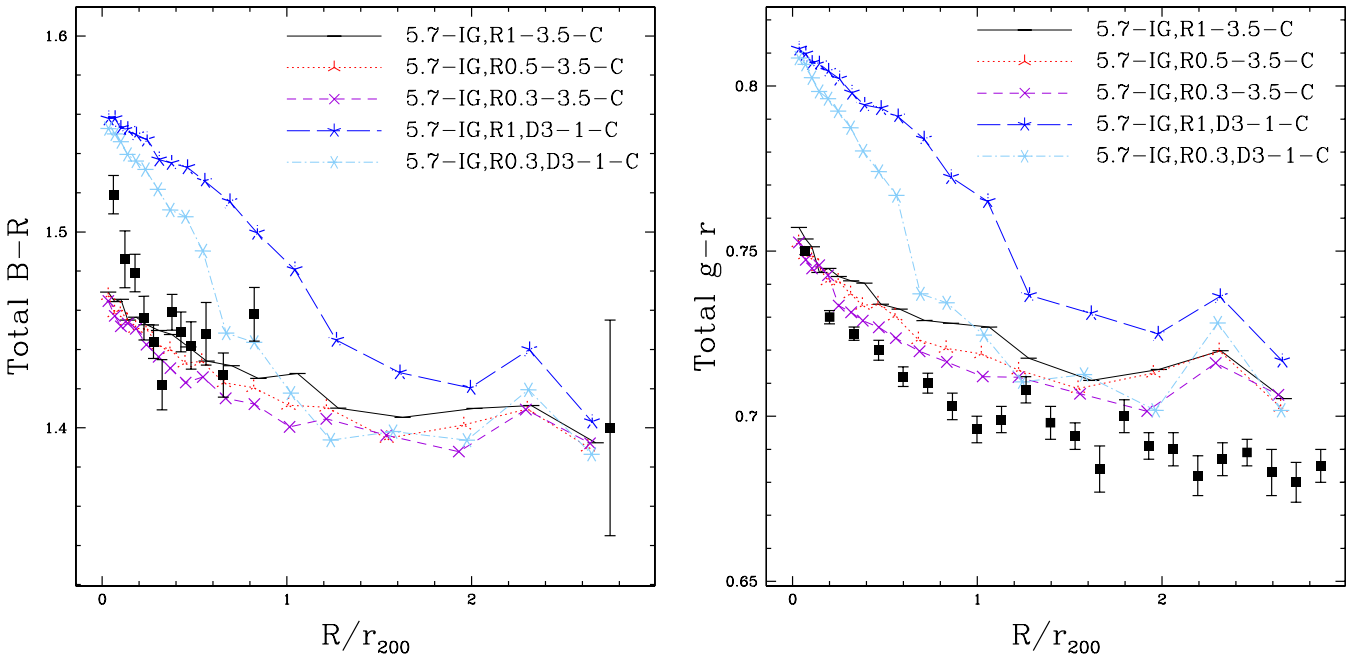

Figure 7. As in Fig. 6, but now for total colours rather than disc colours. All models except the delayed-then-rapid quenching models produce similar (but slightly shallower) slopes and appropriate intercepts, after correcting for excessive reddening in the bulge. Observed colours are redder than the models in the innermost regions, as observed galaxies have higher B/T close to the cluster core, whereas this trend is much weaker in the models. The fact that the trends are similar in slope (but weaker overall) than those for disc colours in Fig. 6 demonstrates that the total colours are consistent, but also that disc colours provide superior constraints on quenching models, being independent of bulge fractions.

by a central face-on opacity $\tau_B^f \sim 4$ in the models of Tuffs et al. (2004). It is well known that spiral galaxies in clusters are stripped of H I (Solanes et al. 2001). If dust is also stripped, then this would introduce a difference in colour solely due to the absence of dust in the clusters compared to its presence in field galaxies. Using the models of Tuffs et al. (2004), we estimate that if all the dust was completely stripped, the effect on disc colour would be to make the discs bluer by 0.10 to 0.22 mag in $B - R$ (with a median of 0.14 for a typical disc with an inclination $i = 60^\circ$). Moreover, if the discs on the outskirts were not stripped (and hence contained dust and were redder) and the ones in the centre were stripped (and hence bluer), then the effect would be to make observed gradients shallower. Thus, it is possible that the intrinsic (dust-free) cluster-centric gradient in disc colour is considerably steeper than the observed one.

There are, however, two arguments against such an extreme scenario. First, according to the models of Tuffs et al. (2004), the bulge light (and bulge colour) are also strongly affected by dust. If the dust is stripped then the bulge will also appear bluer, and more so for bulges than for discs. In their models, for a typical galaxy with a disc inclination of $i = 60^\circ$ the bulge is reddened by 0.35 mag. Thus, if stripping were important, we would expect bulges in the cluster core to be bluer than those at the cluster edges by 0.35 mag. Yet Hudson et al. (2010) show that there is no gradient in bulge colour as a function of cluster-centric radius in NFPS data; SDSS bulges are slightly bluer near the cluster core, but the trend is weak. While it remains possible in principle that an intrinsic dependence of bulge stellar populations exactly cancels the putative 'dust removal' gradient, this seems rather contrived. Rather it suggests that the dust is not stripped in the cluster core.

Secondly, it is also possible to study dust stripping directly. Cortese et al. (2010) studied dust stripping in Virgo. They found that there was evidence of dust stripping from the outer edges of discs, but the amount of dust stripping was high only in the most extreme 'H I-deficient' galaxies (defHI >1). Galaxies with such high levels of H I-deficiency are very rare in rich clusters, comprising only a small fraction of the spiral galaxy population (Solanes et al. 2001). We conclude that there is no strong evidence for dust stripping due to the cluster environment in the bulk of the infalling spiral population. Nonetheless, we can also address this concern by comparing model predictions with measures less sensitive to dust properties, such as line index gradients.

5 COMPARISON WITH STELLAR ABSORPTION LINE INDICES

Stellar absorption lines can yield information on the ages and metallicities of non-star-forming stellar populations. In particular, the strength of the Balmer absorption lines are sensitive to stellar populations that are ∼0.5–2 Gyr old, where colours may not discriminate well. In this section, we will compare the models to the NFPS data for red (i.e. non-star-forming) galaxies only. Note that the NFPS spectra are fibre-spectra of the central regions (2 arcsec diameter fibres). We can predict how much of the light within this central aperture arises from the bulge, and how much is from the disc, by using our bulge/disc model. This calculation has been done by Hudson et al. (2010, see their appendix A1) who derive an 'aperture' B/T as a function of σ, which ranges from 75 to 100 per cent (depending on velocity dispersion) for the NFPS sample. We adopt their empirical scaling here: σ: $B/T = 0.5 \times \log(\sigma_\star) - 0.24$, with the same slope as for B/T_R but a larger intercept, so that 100 km s^{-1}dispersion galaxies have 76 per cent bulge light and 300 km s^{-1}giants are entirely bulge dominated within the fibre aperture. Given the fraction of light in the fibre from the bulge and from the disc, we simulate the central spectral line indices observed by NFPS.

The NFPS line index data are for red galaxies only. To exclude the blue cloud in our models, we reject model galaxies bluer than 0.2 mag from the red sequence, which is assumed to have a slope of 0.05 mag^{-1}. In practice, the line index strengths themselves are only weakly dependent on bulge fraction prescriptions (since fibre bulge fractions are so large). However, line-strength trends are sensitive to the photometric bulge fraction prescriptions. Photometric bulge fractions are typically only 50–60 per cent, and so total colours and hence the colour selection are sensitive to both the disc and bulge models and the photometric bulge fractions in both passbands (B and R).

The relation between projected position and median line-strength indices is shown in Fig. 8. Most of the best-fitting disc models generate comparable gradients. The colour cut – galaxies bluer than 0.2 from the red sequence – is necessary to exclude star-forming galaxies with emission filling in stellar absorption lines. Unfortunately, this cut also only leaves measurable trends for galaxies nearest to the red sequence, which tends to be similar in most models. The 'delayed-then-rapid' quenching model produces the weakest Hβ trend, but both trends are not significantly weaker than for the preferred 5.7-IG,R1-3.5 model. Only the model without pre-processing creates a distinct trend, having the largest slope in both lines – still, only the Hγ trend appears significantly steeper than the data. Thus, like total colours, the line indices do not appear to be a strong constraint on disc quenching models, which is perhaps not surprising given the large fibre bulge fractions and the necessary exclusion of star-forming galaxies.

6 DISCUSSION

We have shown that models with rapid quenching fail to match the observations. Models with 'abrupt' quenching, corresponding to $\tau_{\rm post} = 0$, produce discs which are redder than observed, and a cluster-centric radial gradient in disc colours which is too steep (see Appendix A for full details). This is true almost regardless of the details of the model, and is a result of the large infall times for galaxies near the cluster centre (Fig. 1). A typical galaxy in the cluster core has been a cluster member for at least 7 Gyr. If a galaxy disc is abruptly quenched, its colours will fade to typical values of $B - R = 1.6$ and $g - r = 0.8$ within 1–2 Gyr, whereas median disc colours near the cluster core are $B - R = 1.4$ and $g - r = 0.7$. Thus, the majority of galaxies cannot have been abruptly quenched shortly after infall and must still have some residual star formation, or their disc colours will be too red. The only alternatives are for AQ to be delayed for at least 6 Gyr after infall, or for AQ to only affect a minority of galaxies.

Models in which star formation is quenched more slowly (3–3.5 Gyr) produce shallower disc colour cluster-centric radial gradients and slightly steeper absorption line gradients, in accordance with observations (Fig. 5). We have also found that models incorporating pre-processing in groups of total mass $M > 10^{13}$M$_\odot$ more accurately reproduce the shallow slope of disc colour trends (Fig. 6).

Several recent studies (Weinmann et al. 2010; Wetzel et al. 2013) have attempted to reproduce the observed bimodality in sSFRs in SDSS galaxies with (respectively) full semi-analytic models or simple parametric star formation models. The generally favoured model with $\tau_{\rm post} \sim 3.5$ Gyr does not produce a strong bimodality in disc or global galaxy colours as a result of the relatively long e-folding time. For this reason, the models of Wetzel et al. (2013) prefer a

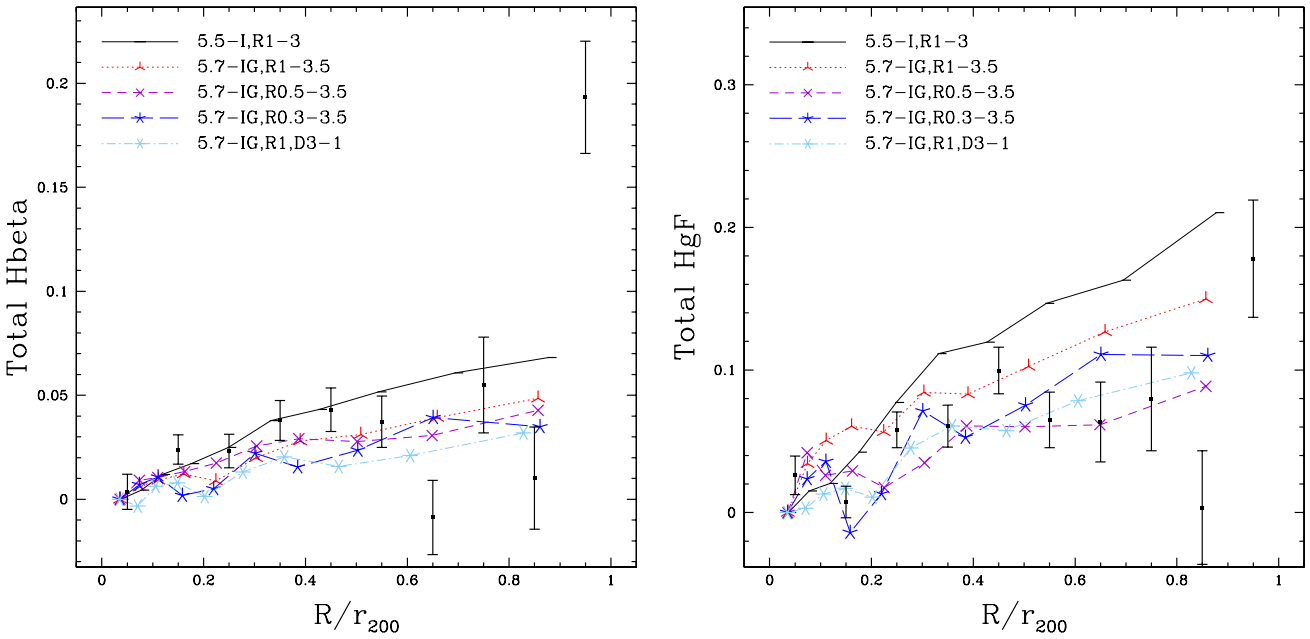

Figure 8. Balmer line-strength index gradients for bulge+disc models, including models with group pre-processing. Virtually all models are consistent with the Hβ and Hγ gradients, given the large error bars. Most models produce very similar slopes, except for the model without pre-processing, which shows the strongest trends.

short quenching *e*-folding time, equivalent to our $\tau_{\rm post}$. To avoid producing too many red galaxies, they introduce an ∼3 Gyr delay before quenching begins.

However, Fig. 6 shows that models with a delay time and a short $\tau_{\rm post}$ also produce discs in cluster centres that are too red compared to those at the virial radius. As an alternative to the quenching delay, we presented models where quenching occurs only within a smaller radius, e.g. 0.3 or $0.5R_{200}$. These models allow a greater fraction of galaxies to remain un-quenched (and hence blue) for longer, because some galaxies will have orbits whose pericentres fall outside the quenching radius on first passage but which, due to dynamical friction, will only pass within the quenching radius on a later pericentre. Fig. 1 suggests that second pericentric passages occur 2–5 Gyr after infall, similar to the 3 Gyr delay required by Wetzel et al. (2013).

One physically motivated alternative to the delay time is to apply quenching at pericentre, where the intracluster medium is densest and tidal forces may be strongest, instead of immediately after infall. Typical infall times from r_{200} to pericentre in the main cluster halo are at most 1 Gyr, and can be shorter at early times. We find that this delay has a very modest impact on galaxy colours. Moreover, if the quenching radius is smaller than r_{200}, the delay time will become even shorter. Thus, it is generally difficult to constrain exactly where quenching occurs. If pre-processing is important, then satellites are unlikely to be significantly quenched much further than at r_{200}.

We can compare the quenching times in our best-fitting models to those quoted in other recent works employing environmental quenching. The best-fitting $\tau_{\rm post}$ is generally 3–3.5 Gyr for models without a delay, with or without pre-processing. Wang et al. (2007) modelled quenching of satellite galaxies, favouring an *e*-folding time (i.e. $\tau_{\rm post}$) of 2.5 Gyr, similar to our own best fits. De Lucia et al. (2012) presented models suggesting that satellites on average spend 5–7 Gyr within a halo of mass $M > 10^{13}{\rm M}_{\odot}$ before being quenched. This 5–7 Gyr quenching time is not entirely inconsistent with some models depending on when one considers a galaxy to be quenched. For example, in $\tau_{\rm post} = 3$ Gyr models, it would take nearly 7 Gyr for star formation to drop to 10 per cent of its pre-quenching value after reaching pericentre.

There are several other ways in which these studies could be improved. The overmerging problem can be addressed partially with better numerical resolution. More recent halo finding algorithms use particle velocities in addition to positions and binding energies (Oman, Hudson & Behroozi 2013), which can improve estimates of infall and pericentre times and pericentre distances and obviate the need for ad hoc merging prescriptions. Halo velocities can also be used to disentangle projection effects and backsplash galaxies (Mahajan et al. 2011; Oman et al. 2013), though more observations would be required to test that prediction.

We have not attempted to constrain models further on the basis of bimodality in part because the $g - r$ bimodality in massive members of rich clusters is quite weak (Oman 2013). This is not surprising, given that there are far fewer star-forming discs in clusters than in the field, and so the blue peak is much more difficult to detect, if it is there at all. Also, $g - r$ does not cover the 4000Å break; bimodality is more evident in colours that do cover the break, like $u - r$ (Balogh et al. 2004). Wetzel et al. (2013) note much weaker bimodality for massive satellites in their fig. 9. However, they considered a much larger range of host haloes ($M_{200} > 10^{12}{\rm M}_{\odot}$), whereas we have focused exclusively on rich clusters. Wetzel et al. (2013) do note that sSFR bimodalities derived from emission lines are insensitive to halo mass, whereas the $g - r$ bimodality in Oman (2013) is sensitive to environment.

Because of our focus on reproducing mean/median gradients, we did not include many ingredients into our disc models, such as mass-dependent SFRs, and scatter in the SFHs which one might model as variable $\tau_{\rm pre}$. These ingredients would likely help in reproducing the scatter about the mean relations and better reproducing mass-dependent trends, e.g. for dwarfs versus giants, for which we do note substantial differences in the infall history (see below). Another missing ingredient in the models is variable or density-dependent quenching strengths. Quenching mechanisms like ram-pressure stripping can depend strongly on intracluster gas density,

pressure and satellite infall velocity (Gunn & Gott 1972; McCarthy et al. 2008). The inclination of the satellite's disc may also have an impact. These effects could introduce significant scatter in the values of $\tau_{\rm post}$. Indeed, if $\tau_{\rm post}$ depends strongly on $r_{\rm peri}/r_{200}$, disc inclination and/or galaxy mass, this could explain the more extreme observations of ram-pressure stripping in galaxies, which our models suggest are not common. The hydrodynamic simulations of Cen (2014) have found a broad distribution of quenching times in clusters, as well as a hint of bimodality in the quenching times of the most massive satellites. A similar bimodality in $\tau_{\rm post}$ could also produce a bimodality in sSFRs, though $g-r$ and $B-R$ bimodality may remain weak.

Finally, we emphasize that these models are designed and applicable for luminous galaxies in rich clusters. Low-mass haloes have on average fallen in more recently (Fig. 2), and dwarf galaxies show evidence of both recent and AQ (e.g. Boselli et al. 2008; Smith et al. 2009a). Dwarfs typically have stronger gradients in colours, line indices (especially Balmer lines) and ages (Smith et al. 2008, 2012), also implying stronger quenching. Both Oman (2013) and Wetzel et al. (2013) find stronger bimodalities for lower mass galaxies, in $g-r$ and sSFR, respectively.

Despite these caveats, it is rather remarkable that reasonable agreement is found between different models and observational data sets. It is also surprising that models with as few as two free parameters can match galaxy colours and absorption line strengths from cluster centre to outskirts, though simultaneously matching both observations is difficult even if pre-processing is neglected. Nonetheless, all of our successful models favour relatively gentle environmental quenching with time-scales longer than the dynamical time in the cluster and longer than typically quoted for ram-pressure stripping of cold gas discs.

7 SUMMARY

We have constructed a catalogue of subhaloes in DM simulations of four rich cluster of galaxies. By tracking halo orbits, we have demonstrated that the infall history of haloes imprints a relationship between two key parameters (infall time and halo velocity dispersion) of haloes and their projected distance from the cluster centre. By assigning stellar masses to a single galaxy within each halo, we have also been able to test a variety of models for the star formation histories of cluster galaxies. Novel aspects of this analysis are, first, the comparison with stellar absorption line strengths and secondly, the separate consideration of bulge and disc colours, as opposed to global colours. Disc colours have been shown to be better discriminants of star formation models than total colours, because disc colours are most sensitive to environment.

In our best-fitting models, the bulge component of galaxies is quenched 'internally', i.e. its age is not determined by infall into the cluster and can be fit with an old SSP. The observed colours of the discs of field galaxies require that, prior to infall, the SFR declines with a characteristic e-folding time $\tau_{\rm pre} = 5$–6.5 Gyr.

Models with no disc quenching fail to explain the redder colours of discs near the cluster centre. Models with short quenching times produce sharp changes in the median colours of discs and a stronger cluster-centric radial disc colour gradient than is observed, and so even 'delayed-then-rapid' quenching models are disfavoured. Such models also overpredict the strength of the Balmer lines. Instead, we prefer a model in which the disc continues to experience exponentially declining SFR with shorter characteristic $\tau_{\rm post} = 3$–3.5 Gyr. This is suggestive of a gentler mechanism (e.g. 'strangulation') as opposed to rapid ram-pressure stripping of the cold gas. Models where quenching only occurs within $0.5\ r_{200}$ produce better fits to the SDSS and NFPS disc colours.

In conclusion, we have found that although quenching is mild, our data require quenching to occur in cluster galaxies not long after they reach pericentre and on time-scales of about 3 Gyr. Quenching may also take place in smaller clusters and groups, but it is not yet clear whether satellites must pass very close to a massive halo to be quenched, or whether infall anywhere within the virial radius is sufficient.

ACKNOWLEDGEMENTS

DST was supported in this work by the NSERC USRA program and Ontario Graduate Scholarships. MJH and MLB acknowledge support from their respective NSERC Discovery Grants. MLB acknowledges funding from NOVA and NWO visitor grants, which support his sabbatical visit to Leiden Observatory, where this work was completed. RJS was supported for this work by STFC Rolling Grant ST/I001573/1 Extragalactic Astronomy and Cosmology at Durham 2008–2013. The Centre for All-Sky Astrophysics is an Australian Research Council Centre of Excellence, funded by grant CE11E0090. Observational data used in this paper are available as raw imaging data from the NOAO data archives, and as parameters tabulated in the cited references.

REFERENCES

Abadi M. G., Moore B., Bower R. G., 1999, MNRAS, 308, 947
Allanson S. P., Hudson M. J., Smith R. J., Lucey J. R., 2009, ApJ, 702, 1275 (AHS)
Azabaijan K. N. et al., 2009, ApJS, 182, 543
Balogh M. L., Baldry I. K., Nichol R., Miller C., Bower R., Glazebrook K., 2004, ApJ, 615, L101
Balogh M. L., Morris S. L., 2000, MNRAS, 318, 703
Balogh M. L., Navarro J. F., Morris S. L., 2000, ApJ, 540, 113
Baugh C. M., 2006, Rep. Prog. Phys., 69, 3101
Berrier J. C., Stewart K. R., Bullock J. S., Purcell C. W., Barton E. J., Wechsler R. H., 2009, ApJ, 690, 1292
Boselli A., Gavazzi G., 2006, PASP, 118, 517
Boselli A., Boissier S., Cortese L., Gavazzi G., 2008, ApJ, 674, 742
Bower R. G., Lucey J. R., Ellis R. S., 1992, MNRAS, 254, 601
Bruzual G., Charlot S., 2003, MNRAS, 344, 1000
Budzynski J. M., Koposov S. E., McCarthy I. G., McGee S. L., Belokurov V., 2012, MNRAS, 423, 104
Cen R., 2014, ApJ, 781, 38
Chung A., van Gorkom J. H., Kenney J. D. P., Vollmer B., 2007, ApJ, 659, L115
Cole S., Lacey C. G., Baugh C. M., Frenk C. S., 2000, MNRAS, 319, 168
Conroy C., Wechsler R. H., Kravtsov A. V., 2006, ApJ, 647, 201
Cortese L. et al., 2010, A&A, 518, L49
Davies R. D., Lewis B. M., 1973, MNRAS, 165, 231
De Lucia G., Weinmann S., Poggianti B. M., Aragón-Salamanca A., Zaritsky D., 2012, MNRAS, 423, 1277
Diaferio A., Kauffmann G., Balogh M. L., White S. D. M., Schade D., Ellingson E., 2001, MNRAS, 323, 999
Dressler A., 1980, ApJ, 236, 351
Driver S. P., Popescu C. C., Tuffs R. J., Liske J., Graham A. W., Allen P. D., de Propris R., 2007, MNRAS, 379, 1022
Gallagher J. S., III, Ostriker J. P., 1972, AJ, 77, 288
Giovanelli R., Haynes M. P., 1985, ApJ, 292, 404
Graves G. J., Faber S. M., Schiavon R. P., 2009, ApJ, 693, 486
Gunn J. E., Gott J. R. I., 1972, ApJ, 176, 1
Haynes M. P., Giovanelli R., Chincarini G. L., 1984, ARA&A, 22, 445
Hogg D. W. et al., 2004, ApJ, 601, L29
Hubble E., Humason M. L., 1931, ApJ, 74, 43

Hudson M. J., Stevenson J. B., Smith R. J., Wegner G. A., Lucey J. R., Simard L., 2010, MNRAS, 409, 405
Katz N., White S. D. M., 1993, ApJ, 412, 455
Kauffmann G., Colberg J. M., Diaferio A., White S. D. M., 1999, MNRAS, 303, 188
Kauffmann G., White S. D. M., Guiderdoni B., 1993, MNRAS, 264, 201
Klypin A., Gottlöber S., Kravtsov A. V., Khokhlov A. M., 1999, ApJ, 516, 530
Knollmann S. R., Knebe A., 2009, ApJS, 182, 608
Komatsu E. et al., 2011, ApJS, 192, 18
Koopmann R. A., Kenney J. D. P., 2004, ApJ, 613, 866
Kroupa P., 2001, MNRAS, 322, 231
Larson R. B., Tinsley B. M., Caldwell C. N., 1980, ApJ, 237, 692
MacArthur L. A., Courteau S., Bell E., Holtzman J. A., 2004, ApJS, 152, 175
Mahajan S., Mamon G. A., Raychaudhury S., 2011, MNRAS, 416, 2882
Mamon G. A., 1987, ApJ, 321, 622
Mamon G. A., Biviano A., Murante G., 2010, A&A, 520, 30
Maraston C., 1998, MNRAS, 300, 872
Maraston C., 2005, MNRAS, 362, 799
Maraston C., Strömbäck G., Thomas D., Wake D. A., Nichol R. C., 2009, MNRAS, 394, L107
McCarthy I. G., Frenk C. S., Font A. S., Lacey C. G., Bower R. G., Mitchell N. L., Balogh M. L., Theuns T., 2008, MNRAS, 383, 593
McGee S. L., Balogh M. L., Bower R. G., Font A. S., McCarthy I. G., 2009, MNRAS, 400, 937
Merritt D., 1984, ApJ, 276, 26
Miller C. J. et al., 2005, AJ, 130, 968
Moore B., Katz N., Lake G., 1996, ApJ, 457, 455
Moore B., Lake G., Katz N., 1998, ApJ, 495, 139
Navarro J. F., White S. D. M., 1994, MNRAS, 267, 401
Nelan J. E., Smith R. J., Hudson M. J., Wegner G. A., Lucey J. R., Moore S. A. W., Quinney S. J., Suntzeff N. B., 2005, ApJ, 632, 137
Oman K. A., 2013, Master's thesis, University of Waterloo
Oman K. A., Hudson M. J., Behroozi P. S., 2013, MNRAS, 431, 2307
Peng Y.-j. et al., 2010, ApJ, 721, 193
Peng Y.-j., Lilly S. J., Renzini A., Carollo M., 2012, ApJ, 757, 4
Postman M., Geller M. J., 1984, ApJ, 281, 95
Power C., Navarro J. F., Jenkins A., Frenk C. S., White S. D. M., Springel V., Stadel J., Quinn T., 2003, MNRAS, 338, 14
Sandage A., Visvanathan N., 1978, ApJ, 223, 707
Simard L., Mendel J. T., Patton D. R., Ellison S. L., McConnachie A. W., 2011, ApJS, 196, 11
Sivanandam S., Rieke M. J., Rieke G. H., 2010, ApJ, 717, 147
Smith R. J., Hudson M. J., Lucey J. R., Nelan J. E., Wegner G. A., 2006, MNRAS, 369, 1419
Smith R. J. et al., 2004, AJ, 128, 1558
Smith R. J., Lucey J. R., Hudson M. J., 2007, MNRAS, 381, 1035
Smith R. J. et al., 2008, MNRAS, 386, L96
Smith R. J., Lucey J. R., Hudson M. J., Allanson S. P., Bridges T. J., Hornschemeier A. E., Marzke R. O., Miller N. A., 2009a, MNRAS, 392, 1265
Smith R. J., Lucey J. R., Hudson M. J., 2009b, MNRAS, 400, 1690
Smith R. J. et al., 2010, MNRAS, 408, 1417
Smith R. J., Lucey J. R., Price J., Hudson M. J., Phillipps S., 2012, MNRAS, 419, 3167
Solanes J. M., Manrique A., García-Gómez C., González-Casado G., Giovanelli R., Haynes M. P., 2001, ApJ, 548, 97
Springel V., 2005, MNRAS, 364, 1105
Springel V., White S. D. M., Tormen G., Kauffmann G., 2001, MNRAS, 328, 726
Sun M., Donahue M., Voit G. M., 2007, ApJ, 671, 190
Taranu D. S., Dubinski J., Yee H. K. C., 2013, ApJ, 778, 61
Thomas D., Maraston C., Bender R., 2003, MNRAS, 339, 897
Tormen G., 1997, MNRAS, 290, 411
Tormen G., Diaferio A., Syer D., 1998, MNRAS, 299, 728
Trujillo-Gomez S., Klypin A., Primack J., Romanowsky A. J., 2011, ApJ, 742, 16
Tuffs R. J., Popescu C. C., Völk H. J., Kylafis N. D., Dopita M. A., 2004, A&A, 419, 821
van den Bosch F. C., Aquino D., Yang X., Mo H. J., Pasquali A., McIntosh D. H., Weinmann S. M., Kang X., 2008, MNRAS, 387, 79
von der Linden A., Best P. N., Kauffmann G., White S. D. M., 2007, MNRAS, 379, 867
Wang L., Li C., Kauffmann G., De Lucia G., 2007, MNRAS, 377, 1419
Weinmann S. M., Kauffmann G., van den Bosch F. C., Pasquali A., McIntosh D. H., Mo H., Yang X., Guo Y., 2009, MNRAS, 394, 1213
Weinmann S. M., Kauffmann G., von der Linden A., De Lucia G., 2010, MNRAS, 406, 2249
Wetzel A. R., Tinker J. L., Conroy C., 2012, MNRAS, 424, 232
Wetzel A. R., Tinker J. L., Conroy C., van den Bosch F. C., 2013, MNRAS, 432, 336
Yagi M., Komiyama Y., Yoshida M., Furusawa H., Kashikawa N., Koyama Y., Okamura S., 2007, ApJ, 660, 1209
Yoshida M. et al., 2008, ApJ, 688, 918

APPENDIX A: SIMPLE MODELS AND THE EFFECTS OF MERGERS

In Section A, we presented basic methods for simple, single-component models based on either internal quenching or environmental quenching. We will now show the results of these models compared to observed trends in total, disc and bulge colours.

Similarly, Section 2.1 presented a method for recovering over-merged orphan haloes also recovered some genuine mergers. We identified candidate mergers using a somewhat arbitrary cut on distance (75 kpc) and binding ratio ($v/v_{\rm escape} < 0.1$) to a more massive halo. We will now show the effects of this merger prescription on predicted colours for single-component models.

Colours for three single-component models are shown in Fig. A1. The three models are an internally quenched SSP, and two 'abruptly quenched' (i.e. $\tau_{\rm post} = 0$) models with constant SFR prior to quenching (i.e. $\tau_{\rm pre} = \infty$). The first model is quenched at infall past r_{200} (I-AQ) while the second is quenched at pericentre (P-AQ). The internally quenched model produces extremely red colours – even redder than bulge colours – and virtually no position-dependent trend, and so can only be considered a possible fit for bulge colours, not disc or total colours. The environmentally quenched model can produce a wide range of trends in colours, but must be tuned to fit observed trends in disc colours. Pericentre quenching can alter the behaviour of the models at intermediate positions ($0.2 < R/r_{200} < 0.8$) but does not alter the overall slope of the relation even in rather extreme model. We conclude that these models are overly simplistic, justifying the use of two-component models in Section 4.4.

We now return to the merger prescription. Depending on the model, the fraction of bright, potentially merged galaxies is about 30–40 per cent. Fig. A1 shows the results of including or potentially merged haloes in single-component models (models including likely mergers are labelled '+Merged'). The differences are small, even for the most extreme AQ models, and excluding potential mergers generally makes median colours bluer, suggesting that candidate mergers are less likely to have been quenched than the remaining haloes.

The mass-quenched/bulge model is insensitive to the exclusion of candidate mergers. Two-component models are generally heavily weighted to the bulge component, so the effects on realistic bulge+disc systems are also much smaller than the offsets shown for a purely infall-quenched system. In summary, the effects of mergers are mainly to change the number of galaxies. Mergers have little impact on disc colours and a negligible impact on total colours.

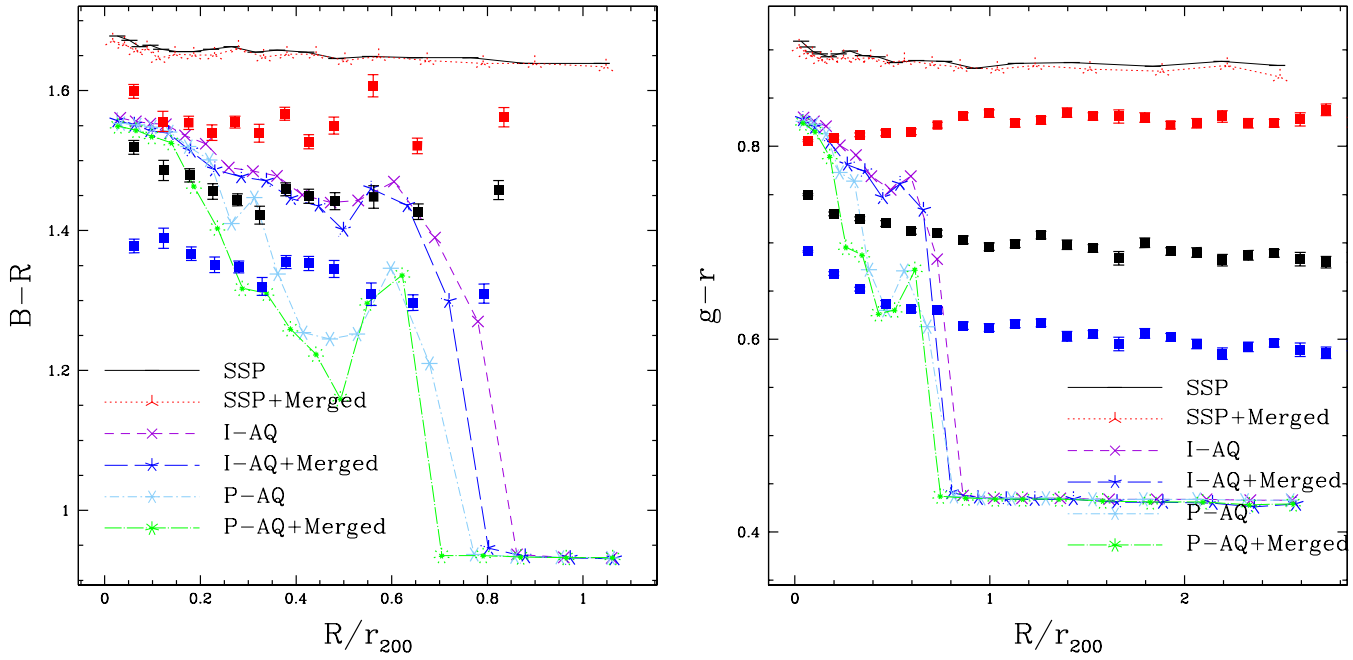

Figure A1. Simple, single-component star formation models described in Section 4.3, compared to NFPS $B - R$ colours (left) and SDSS $g - r$ (right). Observational data are median colours for bulge (red, uppermost values), disc (blue, lowest values) and total (black, middle values), with error bars representing errors on the medians in each bin. Three models are shown – an old, single stellar population (SSP) and two models with constant SFRs prior to infall followed by instant 'abrupt' quenching (i.e. $\tau_{\rm pre} = \infty$, $\tau_{\rm post} = 0$). The I-AQ model is quenched upon infall within r_{200}, while the P-AQ model is quenched at pericentre. Relations are also shown for models including likely mergers ('+Merged'). Candidate mergers are predominantly blue, so including these galaxies makes median colours at a fixed position slightly bluer, or equivalently, shifts the transition to blue-sequence-dominated medians inwards. The effects are not large for infall-based models and negligible for mass-quenched models (bulges)

This paper has been typeset from a TEX/LATEX file prepared by the author.